



HAL
open science

Paleo-ecological quality status induced by natural and anthropogenic impacts in the last 2000 years: a multidisciplinary approach in the outer region of Sepetiba Bay (SE Brazil)

Murilo Barros Saibro, Maria Virgínia Alves Martins, Rubens Figueira, Egberto Pereira, Heitor Evangelista, Marcus Vinícius Licínio, Josefa Varela Guerra, Felipe de Castro Figueiredo Simões, Vincent Marcel Pierre Bouchet, Fabio Francescangeli, et al.

► To cite this version:

Murilo Barros Saibro, Maria Virgínia Alves Martins, Rubens Figueira, Egberto Pereira, Heitor Evangelista, et al.. Paleo-ecological quality status induced by natural and anthropogenic impacts in the last 2000 years: a multidisciplinary approach in the outer region of Sepetiba Bay (SE Brazil). *Journal of Soils and Sediments*, 2024, 24 (11), pp.3722-3749. 10.1007/s11368-024-03925-4 . hal-04813767

HAL Id: hal-04813767

<https://hal.science/hal-04813767v1>

Submitted on 4 Dec 2024

HAL is a multi-disciplinary open access archive for the deposit and dissemination of scientific research documents, whether they are published or not. The documents may come from teaching and research institutions in France or abroad, or from public or private research centers.

L'archive ouverte pluridisciplinaire **HAL**, est destinée au dépôt et à la diffusion de documents scientifiques de niveau recherche, publiés ou non, émanant des établissements d'enseignement et de recherche français ou étrangers, des laboratoires publics ou privés.



Distributed under a Creative Commons Attribution 4.0 International License



Paleo-ecological quality status induced by natural and anthropogenic impacts in the last 2000 years: a multidisciplinary approach in the outer region of Sepetiba Bay (SE Brazil)

Murilo Barros Saibro¹ · Maria Virgínia Alves Martins^{1,2} · Rubens Figueira³ · Egberto Pereira¹ · Heitor Evangelista⁴ · Marcus Vinícius Licínio⁵ · Josefa Varela Guerra⁶ · Felipe de Castro Figueiredo Simões^{1,6} · Vincent Marcel Pierre Bouchet⁷ · Fabio Francescangeli⁸ · Fabrizo Fontalini⁹ · Paulo Alves de Lima Ferreira³ · Ana Beatriz Ramos de Oliveira¹ · Fabricio Leandro Dasmaceno¹ · Thaise Senez-Mello¹ · Grazielle Arantes Reis¹ · Silvia Helena Mello Sousa³ · Rodolfo Dino¹ · Antonio Tadeu dos Reis⁶ · João Wagner de Alencar Castro¹⁰ · Fernando Rocha²

Received: 21 June 2024 / Accepted: 12 October 2024 / Published online: 31 October 2024
© The Author(s) 2024

Abstract

Purpose Some marine organisms can be used as Biological Quality Elements to estimate the degree of environmental impact and to monitor the health of benthic habitats. Organisms with mineralized protections, such as benthic foraminifera, can provide helpful information on the evolution of the coastal system over a long period and determine the Paleo-Ecological Quality Status (Paleo-EcoQS). This work aims at reconstructing the Paleo-EcoQS in the heavily anthropized Sepetiba Bay (SB; Rio de Janeiro State, SE Brazil).

Materials and methods This work is based on a multiproxy approach, including textural, geochemical, and foraminiferal data along the core SP11 retrieved near the Pico da Marambaia (a mountain on the tip of the Marambaia Barrier Island). Geochemical analyses encompassing total organic carbon (TOC), total sulfur (S), total nitrogen (N), calcium carbonate (CaCO₃), stable isotopes in organic matter ($_{OM}\delta^{13}C$, and $_{OM}\delta^{15}N$) and elemental concentrations as well as ²⁰¹Pb, ¹³⁷Cs, and radiocarbon dating were performed to characterize the Paleo-EcoQS in the bay.

Results The values of the Paleo-EcoQS.st (standardized Paleo-EcoQS) index in core SP11 indicate that the paleoenvironmental quality varied from moderate to good between ≈50 AD and ≈1500 AD and from good to high between the ~1920s and ~1990s. Since the 1990s, the Paleo-EcoQS.st has deteriorated considerably, probably due to the deposition of contaminated dredging material in nearby areas. Ballast water discharge may have introduced alien species, such as *Ammonia buxasi*, into the SB.

Conclusions The results obtained in core SP11, compared to those of another core (i.e., SP8) from a nearby area, suggest that the reference level of maximum environmental quality is not always reached in a period before industrialization in coastal ecosystems with significant interaction with the ocean; natural factors, related, for example, to sedimentary dynamic processes or geomorphological changes, can lead to unexpected results.

Keywords Foraminifera · Metals · Geochemical Proxies · Pollution · Alien Species · Ecological Indices

1 Introduction

Approximately half the world's population lives in coastal zones where large metropolitan areas are located. These environments, with their high population density and the occurrence of many activities, are, therefore, commonly highly impacted (Diaz and Rosenberg 2008).

Responsible Editor: Elena Romano

Extended author information available on the last page of the article

The release of sewage effluents and domestic and industrial wastes are among the leading causes of environmental degradation in marine environments (Tsujiimoto et al. 2006; Castelo et al. 2021a; Yuan et al. 2021; Silva et al. 2022a, b; Li et al. 2023). Noticeably, the benthic community composition and structure of coastal ecosystems are largely conditioned by environmental conditions (Tsikopoulou et al. 2019; Dreujou et al. 2021), human activities and climate change (Sandra and Carcedo 2013; Ford et al. 2020). Pollution largely affects the abundance, diversity and biomass of these communities (Dewenter et al. 2023; Sonkoly et al. 2019).

Some marine organisms can be used as Biological Quality Elements (BQEs) to understate the degree of environmental impact and to monitor the health of benthic habitats, i.e., the Ecological Quality Status (EcoQS). Organisms with mineralized protections (i.e., shell or test) have a high preservation potential in sediment records. They can further provide helpful information on the evolution of the coastal system over a long period and determine the Paleo-EcoQS. Foraminifera, ostracods and diatoms have been studied for this purpose, given their high preservation capacity and high abundance in the sedimentary record and their sensitivity to the physical–chemical variations of the environment (Irizuki et al. 2015; Martins et al. 2020; Barik et al. 2022; Song et al. 2022). For instance, fossil benthic diatoms allowed Clarke et al. (2003) to reconstruct 150 years of the history of coastal eutrophication in Roskilde Fjord, Denmark. It was possible to use fossil benthic foraminifera to assess the effects of a ferromanganese plant and to establish Paleo-EcoQS in the harbor of Boulogne-sur-Mer, France (Francescangeli et al. 2016) and industrial operations and intensification of coastal urbanization in the Santos estuary, Brazil (Jesus et al. 2020).

In Brazil, several coastal areas have experienced accentuated eutrophication, such as Vitória Bay (Martins et al. 2019), Guanabara Bay (Vilela et al. 2014; Baptista Neto et al. 2023), Araruama Lagoon (Laut et al. 2020), Lagoa dos Patos (Niencheski et al. 1994), among others. Due to the significant industrialization in its surroundings since the 1950s, disordered urbanization, intensive agriculture, excessive accumulations of organic matter, and input of potentially toxic elements (PTEs), Sepetiba Bay is also a highly contaminated coastal system (Rodrigues et al. 2020; Carvalho et al. 2021; Souza et al. 2021; Silva et al. 2022a). Indeed, developing port activities in this region has led to the introduction of invasive species from ships' ballast water (Damasceno et al. 2024a; Soares et al. 2024). Allochthonous species (e.g., larvae, algae, and protozoa) might settle in the ports of destination, where significant ecological impacts are caused (Bouchet et al. 2023) and can be highly detrimental to the ecosystem balance (Wang et al. 2022). Brazil has a long-lasting tradition of ecological studies on benthic foraminifera (total assemblages or living fauna) (e.g., Soares et al. 2024, and references therein). Furthermore, living foraminiferal fauna performed well in Brazilian systems to evaluate the effects of

different types of pollution, e.g., trace metal elements pollution (e.g., Raposo et al. 2022), organic matter enrichment (e.g., Laut et al. 2024), oil spill (e.g., Nunes et al. 2023), shellfish farming (e.g., Rudorff et al. 2012) and water sewage (e.g., Filippou et al. 2023). Hence, benthic foraminiferal species have the potential to serve as accurate sentinels of the effect of pollution in Sepetiba Bay and to reconstruct Paleo-EcoQS of the bay.

The main objective of this study is to reconstruct the late Holocene environmental changes that occurred in the outer sector of Sepetiba Bay through the analysis of textural, geochemical, and meiofaunal (foraminifera) data along a 127.5 cm long sediment core collected ~25 km away from the current main sources of sediments and pollutants (Fig. 1).

2 Study area

The Sepetiba Bay (herein SB) is a coastal ecosystem located in the Rio de Janeiro state (southeastern Brazil), between 22°54' to 23°04'S and 43°34' to 44°10'W (Fig. 1). It is considered a region of great economic importance due to the presence of two major ports and intense industrial activity, linked to the mining, petrochemical, and steel sectors.

From a geological point of view, SB falls in a region of complex characteristics. On the north, it is bordered by the Serra do Mar hills, which include a set of igneous and metamorphic orogens dating from the Precambrian and raised during the Cenozoic (Zalán and Oliveira 2005). At the south, it is surrounded by a Holocene sandy barrier with an extension of approximately 43 km, while at the west lies a string of islands with migmatitic rocks (Dantas 2000).

The bay is under a tropical humid climatic domain, with low thermal variability, high rainfall during the year, and without dry seasons (Alvares et al. 2013). The hydrographic basin flowing into SB comprises 35 rivers, the most important of which is the Guandú River, responsible for about 86% of the freshwater discharged into the bay (Molisani et al. 2004). The bay has two main connections with the ocean, the most significant in its western portion. In addition, to the east is a narrow tidal channel between Marambaia Barrier Island and the continent. Besides the tidal influence, fluvial discharge and winds shape the water column currents inside the bay (Santos et al. 2018; Carvalho and Guerra 2020).

Due to the scarcity of basic sanitation infrastructure, the growing population, and industrial expansion in areas surrounding the bay, a considerable discharge of organic sewage and potentially toxic elements (PTEs) has negatively affected SB since the 1950s (Souza et al. 2021). Among the industries, the Companhia Siderúrgica Ingá Mercantil (Ingá Mercantil Steel Company), located on Madeira Island, was responsible for the irregular dumping of mining tailings rich in Zn and Cd. Even after its deactivation in 1998, it delivered high metal contamination rates into the bay (Araújo et al. 2017a, b). Over the years, the great concern about the environmental quality of SB has

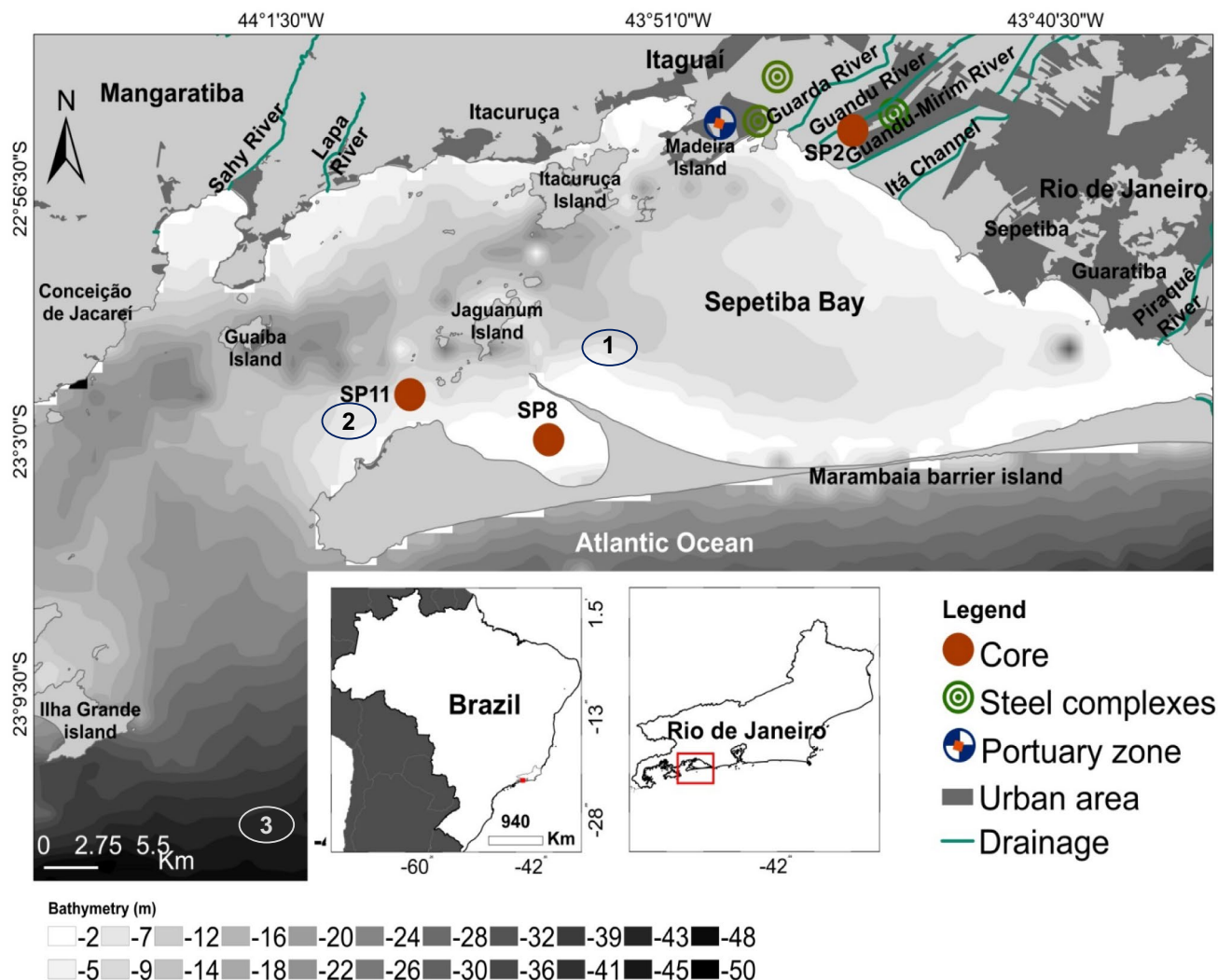


Fig. 1 Study area and location of core SP11. The map also shows the locations of cores SP8 and SP2, discussed in the text. The ellipses 1, 2 and 3 indicate three disposal areas for dredging material in Sepetiba bay (according to Rodrigues et al. 2020). Sites 1 and 2 are located

near the area where the cores SP11 and SP8 (used for comparison) were collected; these sites were used by the Companhia Docas do Rio de Janeiro

motivated several studies (e.g., Barcellos and Lacerda 1994; Lacerda et al. 2004; Souza et al. 2021; Silva et al. 2022a, b). However, it was only recently revealed that there is a tremendous ecological risk in SB (Damasceno et al. 2024a, b, c). This bay has been identified as one of the most contaminated coastal areas in the world (Silva et al. 2022a).

3 Material and methods

3.1 Sampling

This work focuses on a 127.5-cm-long core (SP11; latitude 23°01'47.80 "S, longitude 43°58'00.50 "W; 7.0 m depth) that was collected close to Marambaia Island, in

the outermost portion of SB (Fig. 1). The core SP11 was collected on board a vessel using a Kulleberg-type piston corer in 2022. After collection, the core was stored in a freezer and then opened, described and sampled at 2.5 cm resolution intervals for foraminiferal, textural, and geochemical analyses. Considering the limited diameter of the core (7.5 cm), this thickness (2.5 cm) of the samples made it possible to acquire sufficient samples for the analyses carried out. The core was dated by ^{210}Pb and ^{137}Cs methods and by radiocarbon.

3.2 Core dating

Well-preserved bivalve shells, with both valves and in a living position, were recovered from 92.5 cm and 122.5 cm

layers and selected for radiocarbon analysis. The analyses based on the Accelerator Mass Spectrometry (AMS) method were performed in the Beta Analytic Laboratory (USA). The reported results are accredited to ISO/IEC 17025:2017 Testing Accreditation standards PJLA #59,423. The conventional radiocarbon ages were corrected for full fractionation effects and were calibrated with the BetaCal4.20: HPD method and MARINE20 database (Heaton et al. 2020), according to the probability method of Bronk Ramsey (2009). We applied a DeltaR (ΔR): 67 ± 33 years. The reported $_{OM}\delta^{13}C$ (OM – organic matter) values in organic matter were measured separately on an Isotope Ratio Mass Spectrometer (IRMS).

In addition, the ages of the upper core (0 – 50 cm) were estimated by using the ^{210}Pb and ^{137}Cs dating methods, which have been commonly applied to determine the ages of recent sedimentary strata (< 150 years; Appleby and Oldfield 1978). Samples of about 10 g were collected every 5 cm along the core and then dried and macerated. A high-resolution gamma spectrometry was employed, making use of an extended energy range co-axial hyperpure Germanium (HPGe) detector (model GX5021 – Canberra) with relative efficiency of 50% and resolution of 2.1 keV (FWHM) at the ^{60}Co (1.33 MeV) energy peak. This system was installed inside a shielding with an average thickness of 15 cm and a very low Pb background, internally coated with pure Cu. The detector efficiency curve for the sediment sample was performed using a liquid solution containing a cocktail of radionuclides – National Institute of Standards and Technology (serial number HV951). The cocktail included the radionuclides ^{133}Ba , ^{57}Co , ^{139}Ce , ^{85}Sr , ^{137}Cs , ^{54}Mn , ^{88}Y , and ^{65}Zn . The total counting time for each sample was 24 h. The main radionuclides measured were ^{210}Pb , ^{226}Ra and ^{137}Cs . The geochronological model used the Constant Rate of Supply (CRS).

Chronology is based on the unsupported fraction of the total ^{210}Pb in each stratum as $^{210}Pb_{unsupported} = ^{210}Pb_{total} - ^{210}Pb_{supported}$, where $^{210}Pb_{supported} = ^{226}Ra$. In this model, the mass sediment accumulation rates (SARs) measure the sedimentation along the depth. Sedimentation rates are determined by plotting the log of the excess ^{210}Pb activities against cumulative dry sediment weights and calculating the sedimentation rates over intervals of constant slope. According to Appleby and Oldfield (1983), the age of sediment layers can be obtained from Eq. 1:

$$t = \frac{1}{\lambda} \ln\left(\frac{A_0}{A_x}\right) \tag{1}$$

where A_0 is the total unsupported ^{210}Pb activity in the sediment column, A_x is the total unsupported ^{210}Pb activity in the sediment column beneath depth x , and λ is the radioactive decay of ^{210}Pb (0.03114). In this work, AD calendar ages were used in general.

3.3 Foraminifera

Benthic foraminifera were analyzed from the > 63 μm sediment fraction in 51 sediment layers (2.5 cm thick). Foraminifera were separated from each weighted sub-sample of sediment using a binocular magnifier and an N° 000 mink hairbrush, which was used to isolate the specimens from the sediment and deposit them in foraminiferal micro slides. Specimens were picked and sorted until, ideally, 300 individuals or at least a number greater than 100 specimens were obtained. The density of individuals was determined per gram of bulk sediment (n.°/g). The individuals found were identified whenever possible to species level, with the support of specific references such as Boltovskoy et al. (1980), Loeblich and Tappan (1987), and Disaró et al. (2022). Foraminiferal taxonomy and species names flowed the World Marine Species Database (Hayward et al. 2024). Species richness (SR: number of species per sample) and Shannon Index (H' ; Shannon 1948) were determined.

The diversity $Exp(H'_{bc})$ index, based on Bouchet et al. (2012, 2018), was used to infer the EcoQS along the core SP11. Criteria used to assess the Paleo Ecological Quality Status (Paleo-EcoQS) based on $Exp(H'_{bc})$ ranges were also based on Bouchet et al. (2018).

Ecological Quality Ratio (EQR) was also estimated (Eq. 2). According to Van de Bund and Solimini (2007), the EQR is the ratio between the value of the observed parameter and the expected value under reference conditions:

$$EQR = \frac{Exp(H'_{bc})_{observedvalue}}{Exp(H'_{bc})_{referencevalue}} \tag{2}$$

The EQR varies between 0 and 1. Five class boundaries were 1–0.8 high, 0.8–0.6 good, 0.6–0.4 moderate, 0.4–0.2 bad and 0. 2–0 poor EcoQS (Table 1) were considered following the recommendations of the “Reference Conditions Working Group” of the Water Framework Directive (WFD)

Table 1 Criteria used to assess the Paleo Ecological Quality Status (Paleo-EcoQS) based on $Exp(H'_{bc})$ values (according to Bouchet et al. 2018) and the Paleo-EcoQS.st (standardized Paleo-

EcoQS) based on the EQR ratio or $Exp(H'_{bc})_{st}$ (standardized $Exp(H'_{bc})$) following the recommendations of the REFCOND (2003)

Classification	High	Good	Moderate	Poor	Bad
$Exp(H'_{bc})$	>15	11-15	7-11	3-7	<3
EQR - $Exp(H'_{bc})_{st}$	1.0-0.8	0.8-0.6	0.6-0.4	0.4-0.2	0.2-0.0

(REFCOND 2003). The choice of reference value for this work is analyzed in the discussion section.

3.4 Textural data

Samples for textural analysis were weighed after oven-drying (< 60 °C). The fine sediment was then separated from the sandy fraction by wet sieving on a 63 µm sieve. Each fraction was dried and weighed on a high precision balance.

The fine fraction (< 63 µm) was analyzed in a Malvern Mastersizer 2000 (model hydro 2000MU) in the Laboratory of Geological Oceanography (LaboGeo/UERJ), and the percentages of the fine fractions were determined. The sandy fraction was processed by the classical sieving method, where a series of sieves (2000 µm, 1000 µm, 500 µm, 250 µm, and 125 µm) were stacked and placed on a shaker for 20 min. The textural parameters of the sediment (e.g., mean grain size and sorting) were computed according to Folk and Ward's (1957) methodology.

3.5 Geochemical data

For the determination of total organic carbon (TOC), $\delta^{13}\text{C}_{\text{OM}}$, total sulfur (S) and calcium carbonate (CaCO_3) concentrations, about 3 g of total sediment was separated (at 2.5 cm intervals; 25 samples). The sediments were macerated and sieved on a 63 µm sieve; the sediment was then treated with a 50% diluted HCl in distilled water for 24 h to remove all inorganic carbon. The acid was then removed by five wash cycles with distilled water and dried in an oven at 50°C. The carbonate content was estimated by weight difference.

The TOC and S analyses were performed with LECO SC-632 equipment in the Laboratory of Chemical Stratigraphy and Organic Geochemistry (LGQM) of the Universidade do Estado do Rio de Janeiro (UERJ).

The samples were placed in tin capsules and analyzed using Flash EA 1112 Series and Delta V Advantage equipment in the LGQM (UERJ) to determine stable carbon isotopes in organic matter.

Total nitrogen (N) and $\delta^{15}\text{N}_{\text{OM}}$ values were also determined. For this purpose, about 6 to 8 mg of total sediment was macerated in an agate mortar and analyzed in an Advantage MS Thermo Scientific Delta V (EA-IRMS) coupled to a Costech elemental analyzer at LaQIMar (Laboratory of Marine Inorganic Chemistry, Oceanographic Institute, University of São Paulo, IO-USP).

About 3 g of sediment was separated and macerated in an agate mortar and sieved on a 63 µm sieve for elemental geochemistry analysis (at 2.5 cm intervals; 25 samples). The samples were analyzed at Activation Laboratories Ltd. (Actlabs, Ancaster, Canada). The sediment was digested entirely with a mix of four acids (HNO_3 , HClO_4 , HF, and HCl) and

then analyzed in an Inductively Coupled Plasma-Mass Spectrometry (ICP-MS).

The Enrichment Factor (EF; Eq. 3) (following the formula of Buat-Menard and Chesselet 1979), the Potential Ecological Risk Index (PERI; Swarnalatha et al. 2013; Eq. 4) and the Pollution Load Index (PLI; Tomlinson et al. 1980; Eq. 5) were determined according to the following equations:

$$EF = \frac{\left(\frac{C_x}{C_n}\right)_{\text{Environment}}}{\left(\frac{C_x}{C_n}\right)_{\text{Baseline}}} \quad (3)$$

where C_x corresponds to the concentration of the chemical element in the sample and C_n is the concentration of the normalizing element. In this work, Sc was used as a normalizer element since it generally relates to fine-grained sediments (Castelo et al. 2021a; Silva et al. 2022a, b). Other normalizers are commonly used as a proxy of fine sediment fractions, such as Al, Fe and Li, which are also related to the fine fraction of the sediments (Loring 1991; Birch 2020); however, the concentrations of Sc, a lithogenic chemical element, are not influenced by anthropic activities and have been used with good results in the region (Castelo et al. 2021a; Silva et al. 2022a, b; Damasceno et al. 2024a, b, c).

In the Potential Ecological Risk Index (PERI) equation, the CF is the contamination factor (Håkanson 1980), calculated by the ratio between the concentration of the studied metal and the respective baseline value, estimated by Pinto et al. (2019), based on core SP2 (signed in Fig. 1) and T_{rf} is the toxicity factor of the metal (i.e., Zn = 1; Cr = 2, Co = Cu = Ni = Pb = 5, As = 10, Cd = 30 and Hg = 40; Håkanson 1980; Swarnalatha et al. 2013).

$$\text{PERI} = \sum \text{RI} = \sum (T_{\text{rf}} * \text{CF}) \quad (4)$$

The PERI value is determined from the sum of all the RI values of the potentially toxic elements (PTEs). The Pollution Load Index (PLI) was estimated with the equation (Tomlinson et al. 1980; Eq. 5):

$$PLI = \sqrt[n]{CF_1 \cdot CF_2 \cdot CF_3 \cdot \dots \cdot CF_n} \quad (5)$$

The value PLI is determined by taking the root of “n” (n = the number of metals included in the calculation) and multiplying the contamination factors (CF of each analyzed metal, numbered from 1 to n).

In this work, geochemical ratios, such as Fe/Ca, Ti/Ca, Sr/Ba and V/V + Ni were also used. The Fe/Ca and Ti/Ca ratios were applied to identify the lithogenic sources of sediment introduced in the basin ratios. Iron and Ti are chemical elements commonly found in continental rocks, so their higher concentrations, to the detriment of Ca contents, generally related to marine biogenic components, indicate a period of more significant terrigenous input (Govin et al. 2012).

The Sr/Ba ratio is commonly used to see the influence of fresh and salt water on the system. Strontium is a chemical element mainly linked to biogenic components, such as Ca, and Ba is more abundant in fresh waters. Hence, the variation in the Sr/Ba ratio delimits the records of the influence of continental and oceanic waters (Wang et al. 2021).

The V/V + Ni ratio is usually used to identify changes in sediment oxygenation. Vanadium is a chemical element sensitive to redox conditions, and it deposits close to the bottom in anoxic events, so higher V/V + Ni ratios indicate a more stratified water column (Jones and Manning 1994; Powell et al. 2003).

3.6 Statistical analysis

A Co-inertia analysis (CoIA) (Dolédéc and Chessel 1994) was carried out to identify relationships between the environmental and faunal variables. The CoIA is a multivariate method that identifies trends or co-relationships in multiple datasets that contain the same samples. The CoIA is based on matching a normed PCA on environmental data and a centered PCA on faunistic data (PCA-PCA-CoIA; Dray et al. 2007). A Monte–Carlo test based on 1000 permutations between observations was used to confirm the significance of the Co-inertia result. The environmental dataset was prepared by first conducting a Spearman-based correlation analysis to eliminate redundant variables. For the faunistic dataset, foraminiferal species with an abundance of > 3% in at least one sample were selected. The results have been displayed in three different plots: a) a normed site scores plot showing the position of the sites on the Co-inertia axes using the environmental (origins of the arrows) and faunal (arrowheads) Co-inertia weights (the shorter the arrows, the better the concordance between the two projections); b) canonical weights of the environmental dataset; c) canonical weights of the faunal dataset. Vectors pointing in the same direction are correlated, and longer vectors contribute more to the structure.

Both datasets were logarithmically transformed before statistical analysis ($\log(x + 1)$). Layers 2.5, 45 and 50 were removed because some environmental parameters were not measured, and there were few foraminifera. The statistical test and multivariate analysis were carried out using the software R and the package ade4 (Dray et al. 2007).

4 Results

4.1 Age model

Core SP11 was mainly composed of fine sand with a dark greenish-grey color and some layers containing mollusk shells and fragments with no apparent primary structures. The ^{137}Cs peak from 1963 AD (*Anno Domini*),

corresponding to nuclear weapons tests, was not found in the core. Although the sedimentation rate varied throughout the core (Fig. 2A–C), according to ^{210}Pb and ^{137}Cs results (Appendix 1), the average sedimentation rate every two years (yr^{-2}) was about $0.64 \pm 0.24 \text{ g cm}^{-2} \text{ yr}^{-2}$. The age plot of the sedimentation rate identified two prominent peaks (Fig. 2C): the first in 1996 (22.5–20.0 cm; $1.15 \text{ g cm}^{-2} \text{ yr}^{-2}$) and the second one in 1959 (42.5–40 cm; $0.76 \text{ g cm}^{-2} \text{ yr}^{-2}$); between them, the sedimentation rate was significantly lower (between 0.40 – $0.60 \text{ g cm}^{-2} \text{ yr}^{-2}$).

According to the CRS ^{210}Pb age model, the 52.5–50 cm sediment layer was deposited in 1926 AD. However, radiocarbon ages indicated that the basal part of the core (i.e., 122.5 cm) may be older than 50 AD (Table 1).

4.2 Benthic foraminifera

The foraminiferal density varied between 15–1301 $\text{n.}^\circ \text{ g}^{-1}$ (mean or $\bar{x} = 429 \pm 656 \text{ n.}^\circ \text{ g}^{-1}$; Fig. 3A, Appendix 2). Species richness (SR; $\bar{x} = 39 \pm 32$) and H' ($\bar{x} = 2.9 \pm 0.6$) varied between 12–76 and 2.2–3.3, respectively (Fig. 3A; Appendix 2). A total of 244 species were identified, and an additional six taxa could only be classified up to the order level (Appendix 3). The taxonomic analysis revealed the presence of 94 genera, 46 families, and nine orders across four distinct taxonomic Classes: Monothalamea, Nodosariata, Tubothalamea, and Globothalamea. Globothalamea exhibited the largest identified taxa (206 total), constituting over 80% of the total diversity. Tubothalamea (10.8%) and Nodosariata (6.4%) accounted for 27 and 16 identified taxa, respectively, while Monothalamea (0.4%) comprised only one taxon which was the species *Psammospaera fusca*.

Thirteen species exhibited marked peaks in relative abundance along the core. *Ammonia tepida* recorded the highest peak of relative abundance among all species (60%), followed by *Ammonia parkinsoniana* (40%), *Rosalina williamsoni* (37.2%), *Ammobaculites exiguus* (36.7%), *Cribrorhaphidium poeyanum* (35.5%), *Ammonia rolshauseni* (26.8%), *Elphidium oceanense* (22.5%), *Buccella parkerae* (18.5%), *Pseudonion japonicum* (17.4%), *Buliminella elegantissima* (16.1%), *Rotorbis auberii* (16%), *Globocassidulina crassa* (14.1%) and *Buccella peruviana* (13.6%). Although *A. tepida* showed the highest peak of relative abundance, *R. williamsoni* exhibited the most frequent peaks of abundance.

Four intervals can be recognized along the core SP11 based on foraminiferal distribution (Figs. 3 and 4). The first one, from the core bottom up to 100 cm, was characterized by low foraminiferal density and high epifaunal organisms (Figs. 3 and 4); foraminiferal assemblages were dominated by *R. williamsoni*, *B. peruviana*, and *R. auberii*. The H' and SR indices showed values close to the average in this section (Fig. 3).

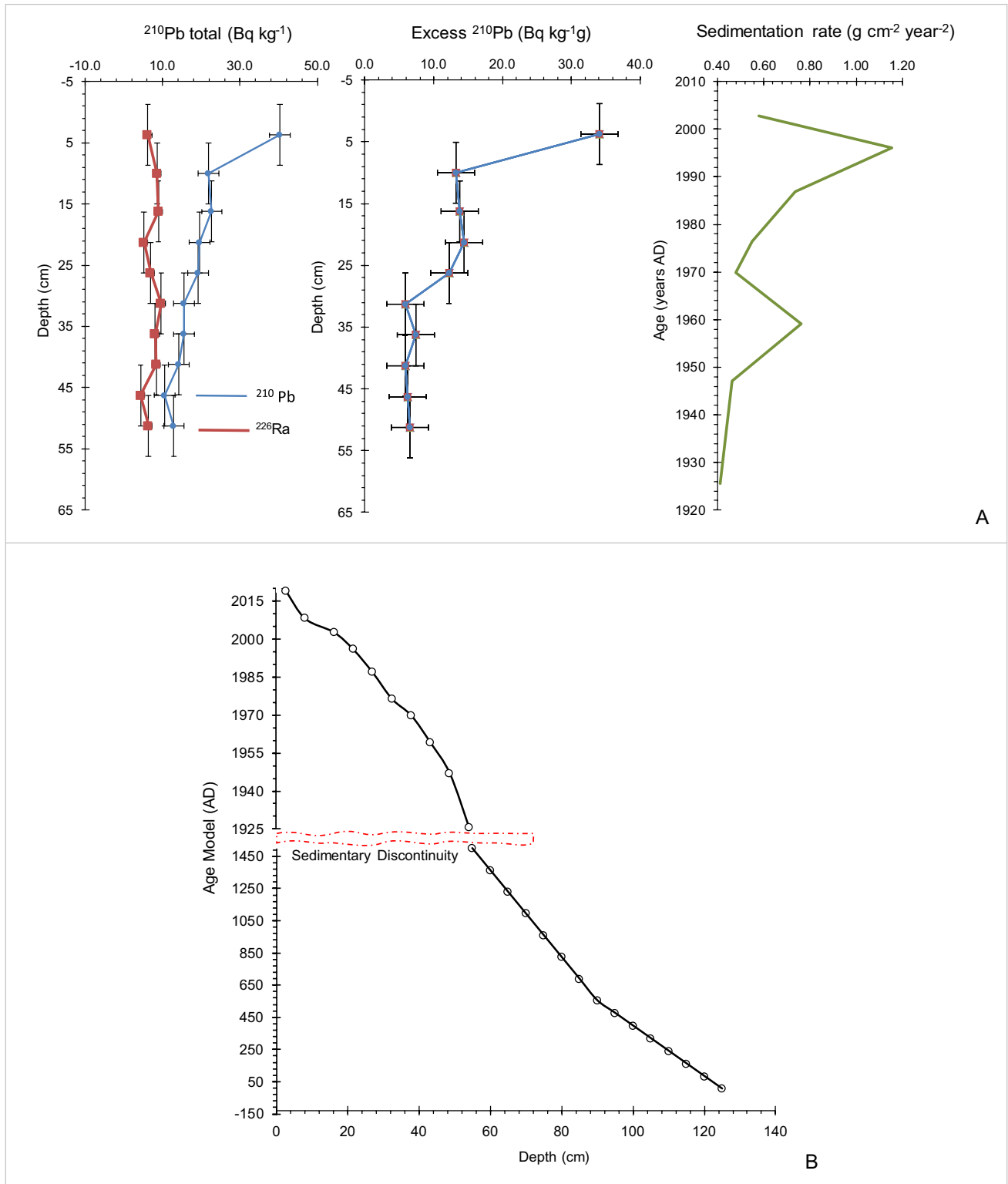


Fig. 2 Depth plots of total ^{210}Pb (Bq kg^{-1}) and Excess ^{210}Pb ($\text{Bq kg}^{-1}\text{g}$) and sedimentation rate ($\text{g cm}^{-2} \text{ year}^{-2}$) for core SP11 based on ^{210}Pb . B. Age model (based on *Anno Domini* – AD) for core SP11 based on CRS ^{210}Pb age model (Appendix 1) and radiocarbon dating (Table 2)

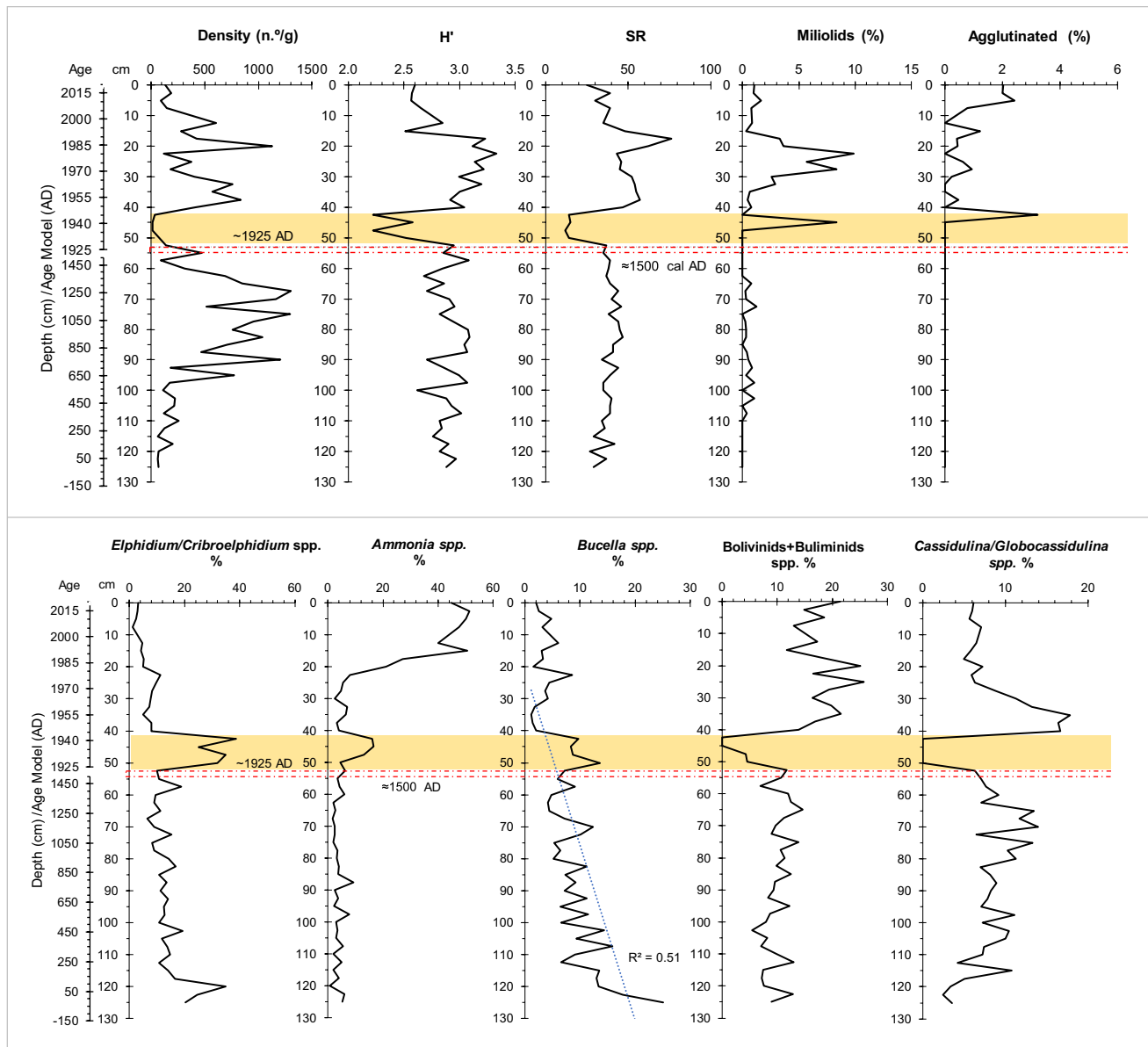


Fig. 3 Depth plots of benthic foraminiferal parameters: density (n° per gram of bulk sediment), Shannon index (H'), species richness (SR), percentage of miliolid and agglutinated specimens and *Elphidium/Criboelphidium*, *Ammonia*, *Buccella*, Boliviniids+Buliminids,

Cassidulina/Globocassidulina taxa. An age scale is represented. The yellow band marks the interval with very low foraminiferal density after a sedimentary discontinuity (marked with red dashes) between ~1500–1925 AD

A significant increase in foraminiferal density accompanied by minor H' and SR changes were documented in the 100–50 cm interval (Fig. 3). *Rosalina williamsoni* remained the dominant species, followed by *B. peruviana* and *R. auberii* (Fig. 4). However, other foraminifera, such as *Globocassidulina crassa* and *Cassidulina braziliensis*, were also observed (Fig. 4).

The foraminiferal density abruptly dropped, reaching the lowest values in the interval between 50 and 40 cm (Fig. 3). This section recorded a significant increase in *Elphidium/Criboelphidium* and agglutinated foraminifera. It was also

marked by the first peak of *Ammonia* and *Quinqueloculina* genera, and the disappearance of *R. williamsoni*, along with many other species (Figs. 3, 4). The percentage of epifaunal species decreased, but an increase in the relative abundance of *B. peruviana*, *P. japonicum*, *A. rolshauseni*, and *Elphidium advenum* was also documented (Fig. 4).

The foraminiferal density and the percentage of epifaunal species increased significantly between 40 and 10 cm but diminished in the uppermost part of the core (10–0 cm; Figs. 3 and 4). In this interval, *R. williamsoni* reappeared with a great abundance at 40 cm but tended to disappear

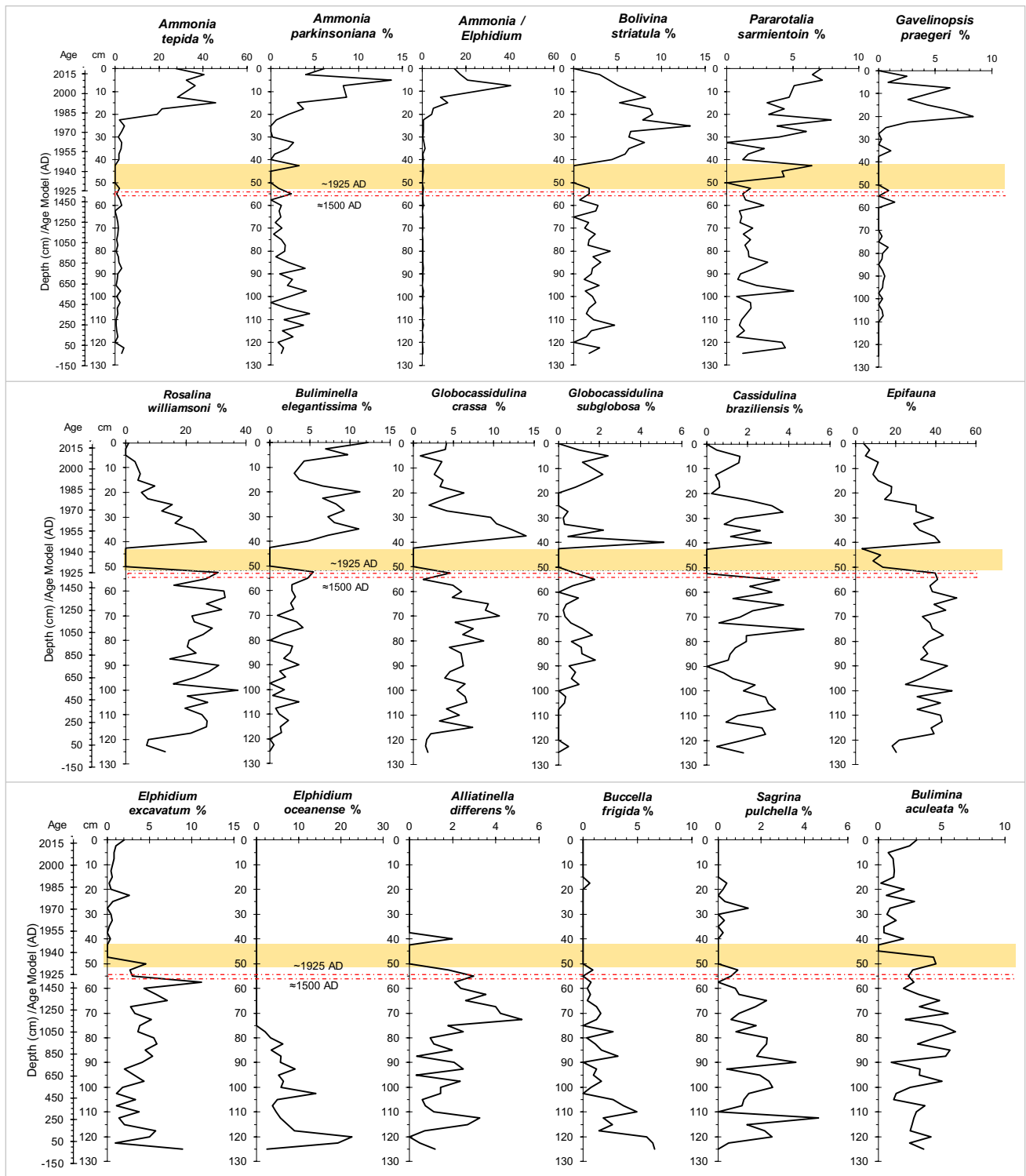


Fig. 4 Depth plots of the main foraminifera species. *Ammonia/Elphidium* ratio and the percentage of epifaunal species are also presented. An age scale is represented. The yellow band marks the inter-

val with very low foraminiferal density after a sedimentary discontinuity (marked with red dashes) between ~1500–1925 AD

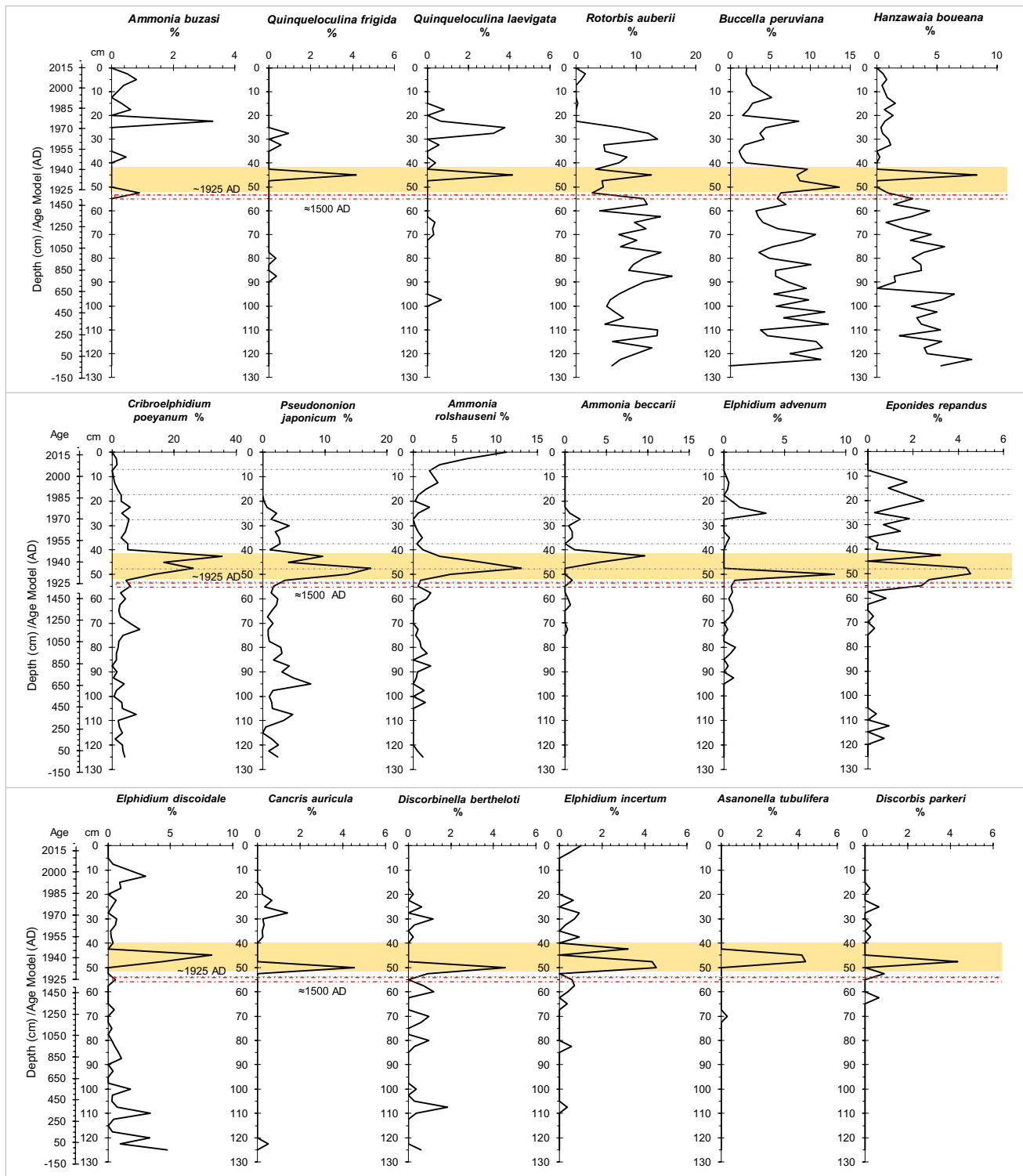


Fig. 4 (continued)

towards the core top (Fig. 4). Epifaunal species and H' and SR indices reached their highest values between 40–20 cm and declined in the uppermost part of the core (Figs. 3, 4). *Ammonia* was the most abundant genus, mainly represented

by *A. tepida*, *A. parkinsoniana*, *A. rolshauseni*, and *Ammonia buzasi* (Figs. 3, 4). Other genera, such as *Bolivina* and *Buliminella*, also had a significant presence between 40–0 cm (Figs. 3, 4).

The foraminiferal density increased significantly from 40–10 cm but reduced in the uppermost part of the core (10–0 cm) and the percentage of epifaunal species (Figs. 3, 4). In this interval, *R. williamsoni* reappeared with a great abundance at 40 cm but tended to disappear towards the top. Epifaunal species reached their highest values between 40–20 cm, where H' and SR reached their highest values of this core (Figs. 3, 4). In the uppermost part (1996–2021) of the core, *Ammonia* was the most abundant genus, mainly represented by *A. tepida*, *A. parkinsoniana*, *A. rolshauseni*, and *A. buzasi* (Figs. 3, 4). Other genera, such as *Bolivina* and *Buliminella*, also had a significant presence between 40–0 cm (Figs. 3, 4).

4.3 Textural data

The core SP11 predominantly comprises very fine and fine sand, and moderately to poorly sorted sediments (Fig. 5; Appendix 4). The core exhibited two distinct coarser intervals where the content of the sand (mainly medium to coarse sand fractions) increased, interspersed by finer layers (Fig. 5; Appendix 4). Sorting values and sediment fractions varied with depth, increasing the complexity of sediment composition (between 25 cm and the top of the core; Fig. 5). Skewness values show a similar pattern to sorting, while kurtosis values tend to be the opposite (Fig. 5). The values of the three main modes vary considerably along the core (Fig. 5).

4.4 Geochemistry

The TOC, S, N, $_{OM}\delta^{13}C$, and $_{OM}\delta^{15}N$ values showed significant changes along the core SP11 (Fig. 6; Appendix 4). The contents of TOC ($\bar{x}=0.53\pm 0.21\%$) and S ($\bar{x}=0.14\pm 0.05\%$) varied between 0.29–0.96% and 0.09–0.3%, respectively. They had relatively lower values in the 115–45 cm interval and increased upwards (Fig. 6).

The $_{OM}\delta^{13}C$ values ($\bar{x}=-22.64\pm 0.79\text{‰}$) oscillated from -24.25‰ to -21.33‰ and showed a trend similar to that of TOC and S (Fig. 6). In the lower interval, below 50 cm, the $_{OM}\delta^{13}C$ values were more negative, becoming progressively more positive towards the core top (Fig. 6).

The C/S ratio values were lower than 3 in most of the core, except in the first 20 cm and around 85 cm (Appendix 4). The concentrations of N ($\bar{x}=0.06\pm 0.03\%$) varied from 0.02 to 0.1%. The lowest N values were determined between 135–85 cm and 65–45 cm, whereas the highest values were found between 85–65 cm and in the upper part of the core, where they tended to increase towards the top (Fig. 6). The $_{OM}\delta^{15}N$ values ($3.26\text{--}6.59\text{‰}$; $\bar{x}=5.56\pm 0.69\text{‰}$) decreased significantly between 95–115 cm and further at 55 cm and 15 cm depth (Fig. 6; Appendix 4).

4.5 Elemental geochemistry

Appendix 4 reports the maximum, minimum, mean, and standard deviation (SD) values of the analyzed chemical elements' concentrations along core SP11. The concentrations of selected chemical elements (Zn, Cd, Pb, P, Mg, Al, Fe, Ca, Mo, and Mn) and geochemical indices (EF-Zn, EF-Cd, EF-Mo, EF-U, and PLI) are shown in Figs. 6 and 7. While, for instance, Zn, Cd, Pb, P, and Mn concentrations tended to increase from ≈ 50 cm to 0 cm, Mg, Mo, and Ca reached higher concentrations in general in the lower core section (Figs. 6 and 7). The EF values of Zn and Cd tended to increase at the core top (Fig. 7). The Al and Fe contents show recurring peaks above the average (Fig. 6). Molybdenum concentrations and EF-Mo and EF-U values rise between 105–60 cm and 20–5 cm (Figs. 6 and 7).

The maximum values of RI were reached for Cd (164.2). The maximum values of PERI and PLI reached 205.1 and 1.8, respectively (Appendix 4). The PLI (Fig. 7) and PERI values tend to increase at the top of the core and follow a pattern similar to those of the concentrations and EF values of Cd and Zn (Fig. 7; Appendix 4).

4.6 Statistical analysis

The results from the CoIA showed that the first and second eigenvalues represent 91.3% of the total variation (Fig. 8A–C). The CoIA analysis compares separated PCAs from environmental and faunal datasets. In Fig. 8B and C represent the scatter plots of the Canonical weight, i.e., the coefficients of the combinations of the variables for each table to define the CoIA axes. In Fig. 8A, the scatter plot of the CoIA analysis represents the score of the core layers. For the interpretation, we can consider that the three plots are overlapped (Fig. 8A–C). In Fig. 8B and C, the position of the core layers depends on both environmental and faunal weights.

In the scatter plot in Fig. 8A, it can be observed that sample layers from 7.5 to 40 were separated from the rest of the samples and were placed at the right of the first axis. These layers are positively related, for example, to PLI, PERI, TOC, EF-Zn and N. Amongst the most abundant and/or frequent species, *A. tepida*, *B. striatula*, *B. elegantissima*, *Pararotalia sarmientoi*, and *Gavelinopsis praegeri*, correlated positively with these variables (PLI, PERI, TOC, EF-Zn and N; Appendix 5) and these layers (Fig. 8B–C). *Elphidium excavatum*, *R. williamsoni*, *E. oceanensis*, *B. peruviana*, *Sagrina pulchella*, *Alliatinella differens*, *Bulimina aculeata*, *Rotorbis auberii* are negatively correlated with PLI, PERI, TOC, EF-Zn and N and positively correlated with relatively coarser sediments (Fig. 8B–C; Appendix 5).

The $\text{Exp}(H'_{bc})$ values in the core SP11 ranged from 14.8–34.4 (21.5 ± 10.0) (Appendix 2).

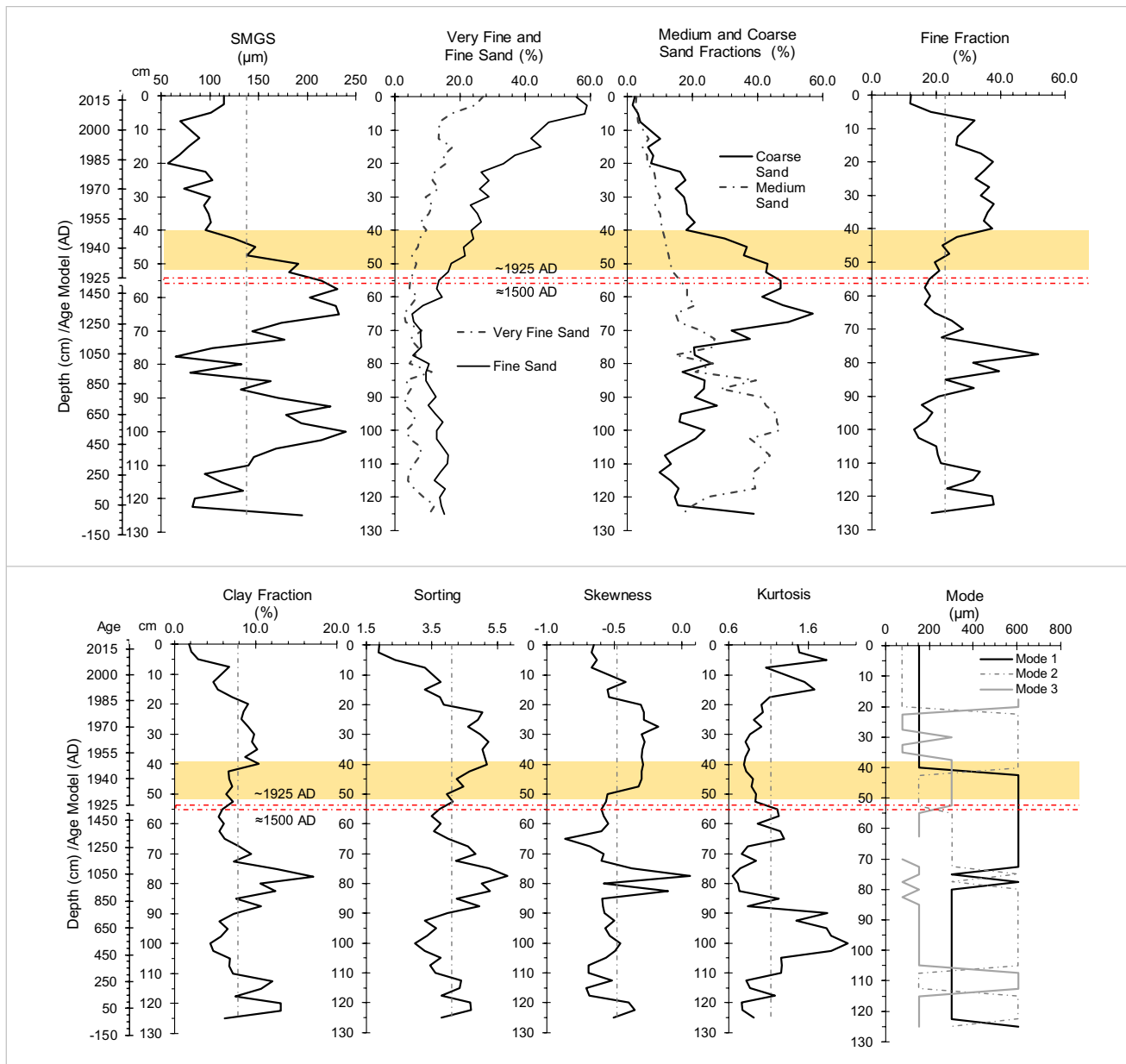


Fig. 5 Depth plots of sediment fractions percentage and values of textural parameters. An age scale is represented. The yellow band marks the interval with very low foraminiferal density after a sedimentary

discontinuity (marked with red dashes) between ~1500–1925 AD. SMGS – sediment mean grain size

5 Discussion

5.1 Reconstructing the sedimentary environment

Based on the sediment mean grain size (SMGS) and Folk and Ward's statistical parameters, core SP11 consists of fine and very fine sands, generally polymodal, and mainly contains poorly and very poorly sorted particles. However, three coarser sections/layers (~125 cm, 110–85 cm, and 70–50 cm) interspersed within the finer-grained intervals

(125–110 cm, 90–75 cm, and 45–0 cm) are identified. The coarser core sections are characterized by a higher proportion of medium (mainly at 110–85 cm) and coarse (mainly at 70–50 cm) sand that has lower sorting values and is more negatively skewed than the surrounding sediments; in these sections, sediments are leptokurtic to mesokurtic (with a higher concentration of coarse particles). These textural characteristics in coarser core sections indicate better sediment sorting, likely due to a reduced deposition of fine particles.

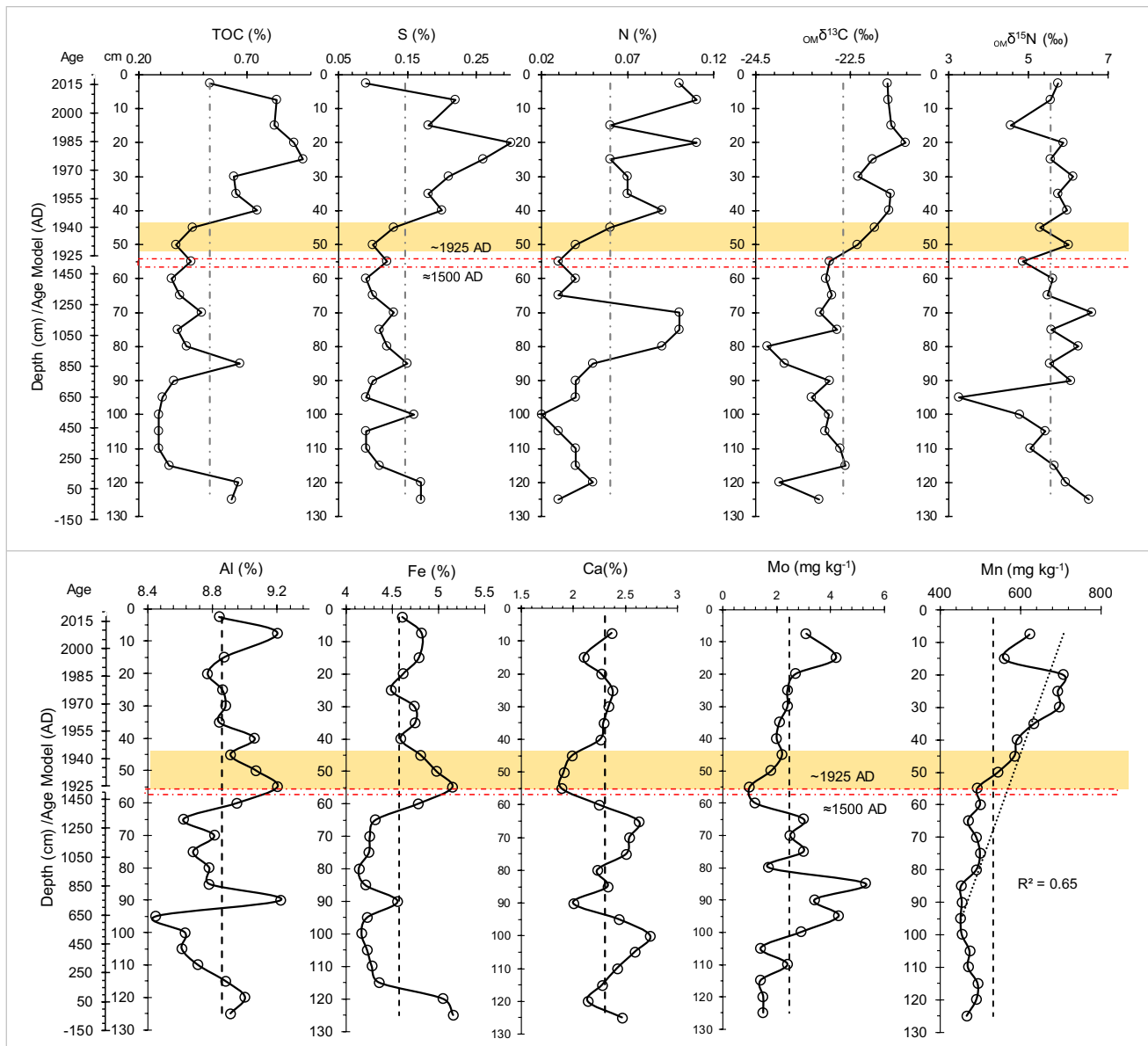


Fig. 6 Depth plots of the percentage (%) of total organic carbon (TOC), total Sulphur (S), total Nitrogen (N) and $OM\delta^{13}C$ and $OM\delta^{15}N$ values (‰) and metals concentrations (Al, Al, Fe, Ca, Mo and Mn).

An age scale is represented. The yellow band marks the interval with very low foraminiferal density after a sedimentary discontinuity (marked with red dashes) between ~1500–1925 AD

The Sr/Ba ratios indicate that these particle-size changes may have occurred in a marine depositional environment (Fig. 9). Core SP11 was collected in the submerged beach where mega-ripple-like structures are noticeable. These sandy structures are dynamic and can migrate depending on the tidal currents and wave influence (Koop et al. 2019; Tholen et al. 2022). This process creates a crest and trough structure, which facilitates the deposition of coarser (crest) and finer (trough) sediments (Koop et al. 2019). The changes in grain size in the core SP11 may be associated with the dynamics of these structures and shifts in the energy

of the sediment transport agent and/or the sedimentation environment.

In addition, processes associated with wave-induced liquefied sediment gravity flow (Fig. 10) may also have contributed to the textural changes in core SP11. These processes occur from the liquefaction of saturated sediment into a fluid induced by waves resulting mainly from large storms (Fig. 10; Yu et al. 2022). With the pressure generated by the sediment load above combined with the saturation of pore water, in moments of storms, part of the sedimentary column is remobilized and slides to the lower regions, carrying

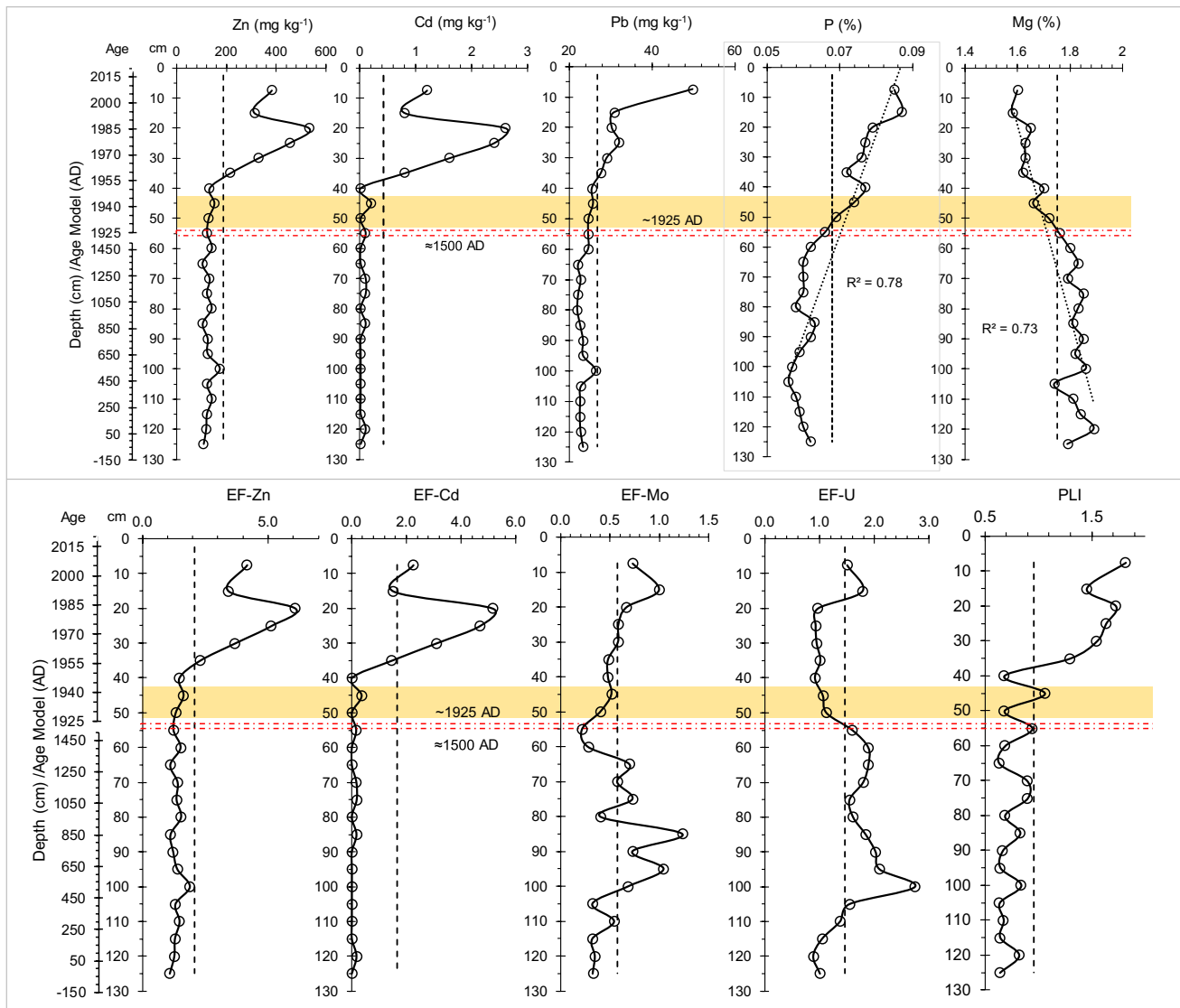


Fig. 7 Depth plots of the concentrations of Zn, Cd, Pb, P and Mg and Enrichment Factor (EF) values for Zn, Cd, Mo, and U, and the pollution load index (PLI). The dashed vertical line represents the average value of the variables. An age scale is represented. The yellow band

marks the interval with very low foraminiferal density after a sedimentary discontinuity (marked with red dashes) between ~1500–1925 AD

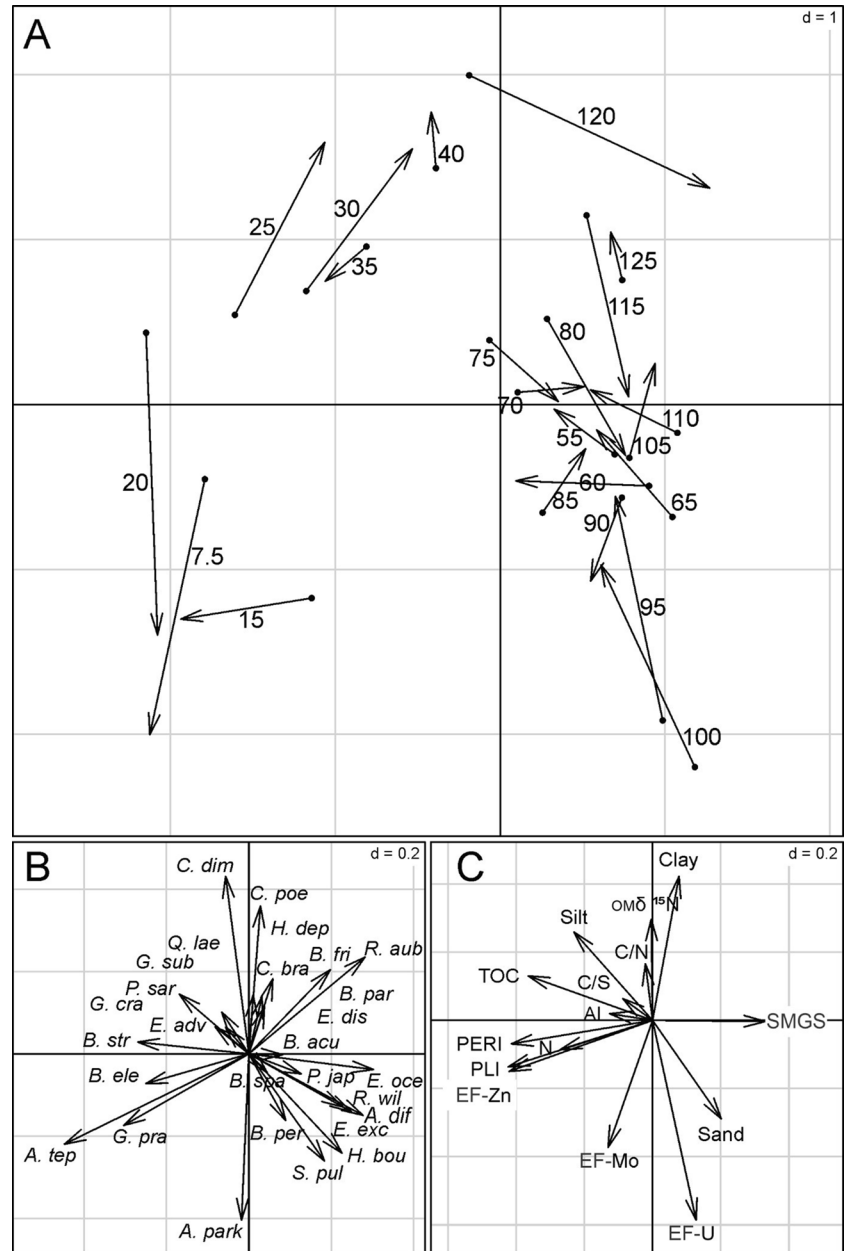
mainly the finest sediment fractions (Tholen et al. 2022; Yu et al. 2022; Fig. 10).

However, the cyclical reduction in Sr/Ba values (Fig. 9) may indicate the presence of less saline waters. Despite the absence of nearby important rivers, which flow mainly into the inner region of Sepetiba Bay, it can be assumed that during periods of high rainfall, the flow of continental freshwater might contribute to the reduction of salinity in this part of the bay; the transport of low salinity waters to the outside area may be facilitated by tidal currents and/or northerly winds. In phases of decreasing Sr/Ba values (indicative of phases of higher rainfall), there are generally peaks in Ti/Ca values (Fig. 9) and Fe/Ca (Fig. 11), which should indicate a

rise in the contribution of terrigenous sediments to the study area. During periods when there is a greater freshwater influence in the study area, there is a tendency for the abundance of euryhaline foraminifera species to increase, such as *E. excavatum*, *A. tepida*, *A. parkinsoniana*, *P. sarmientoi*, *B. elegantissima*, among others.

Based on the ^{210}Pb dating for the upper ~50 cm layer and the radiocarbon dating for the 122.5 cm and 92.5 cm layers (Fig. 2; Table 2), it can be inferred that there was a significant gap in the sedimentary record corresponding to ~400 years before ~1925 AD. Thus, the probable age of the sediments immediately below 50.0/52.5 cm might be ~1500 AD. The sediment loss is probably coeval or after the deposition of

Fig. 8 Coinertia results. Legend: Clay – clay fraction; Sil – silt fraction; $OM\delta^{15}N$ – nitrogen isotope in organic matter; TOC – total organic carbon; Al – aluminum concentrations; N – nitrogen concentrations; EF-Zn, EF-Mo, EF-U—enrichment factors of Zn, Mo and U; C/N—carbon/nitrogen ratio; C/S—carbon/sulfur ratio; PERI—Potential Ecological Risk Index; PLI—Pollution Load Index; A. dif—*Alliatinella differens*; A. park—*Ammonia parkinsoniana*; A. tep—*Ammonia tepida*; B. acu—*Bulimina aculeata*; B. ele—*Buliminella elegantissima*; B. fri—*Buccella frigida*; B. par—*Buccella parkerae*; B. per—*Buccella peruviana*; B. spa—*Bolivina spathulata*; B. str—*Bolivina striatula*; C. bra—*Cassidulina braziliensis*; C. dim—*Cibicides floridanus* var. *diminutivus*; E. exc—*Elphidium excavatum*; C. poe—*Criboelphidium poeyanum*; E. adv—*Elphidium advenum*; E. dis—*Elphidium discoidale*; E. oce—*Elphidium oceanense*; G. cra—*Globocassidulina crassa*; G. pra—*Gavelinopsis praegeri*; G. sub—*Globocassidulina subglobosa*; H. bou—*Hanzawaia boueana*; H. dep—*Haynesina depressula*; P. jap—*Pseudononion japonicum*; P. sar—*Pararotalia sarmientoi*; Q. lae—*Quinqueloculina laevigata*; R. aub—*Rotorbis auberii*; R. wil—*Rosalina williamsoni*; S. pul—*Sagrina pulchella*



coarser sediments between 80–55 cm (Figs. 2, 5). This sedimentary discontinuity was likely caused by coastal erosion associated with strong storm events, leading to a drop in foraminiferal density and diversity (Fig. 3). Sedimentary discontinuities are common features in SB. They are related to geomorphological changes over time due to climatic variations and changes in sea level, the construction and rupture of the Marambaia Barrier Island, and even anthropogenic activities (Borges and Nittrouer 2016; Damasceno et al. 2024c).

After this erosive phase, the study area received an increased deposition of terrigenous sediments, as indicated by the rise in Fe/Ca and Ti/Ca ratios (~50–40 cm; Figs. 9,

11). Both disturbances significantly reduced foraminiferal density and diversity (Fig. 3). After these disturbances, the recovery of the foraminiferal community was slow (Fig. 3).

Other peaks in Ti/Ca and/or Fe/Ca ratios are also observed, such as between ~125–100 cm, ~90–80 cm and ~10–0 cm (Figs. 9, 11), indicating the cyclical arrival of higher terrigenous sediments. This rising contribution of terrigenous sediments commonly occurs concomitantly with the reduction of Sr/Ba values (Fig. 9), indicating a decrease in salinity, probably related to higher rainfall, as mentioned.

The hydrodynamic conditions and degradation processes did not allow for a large preservation of organic matter at the studied site, as indicated by the low TOC

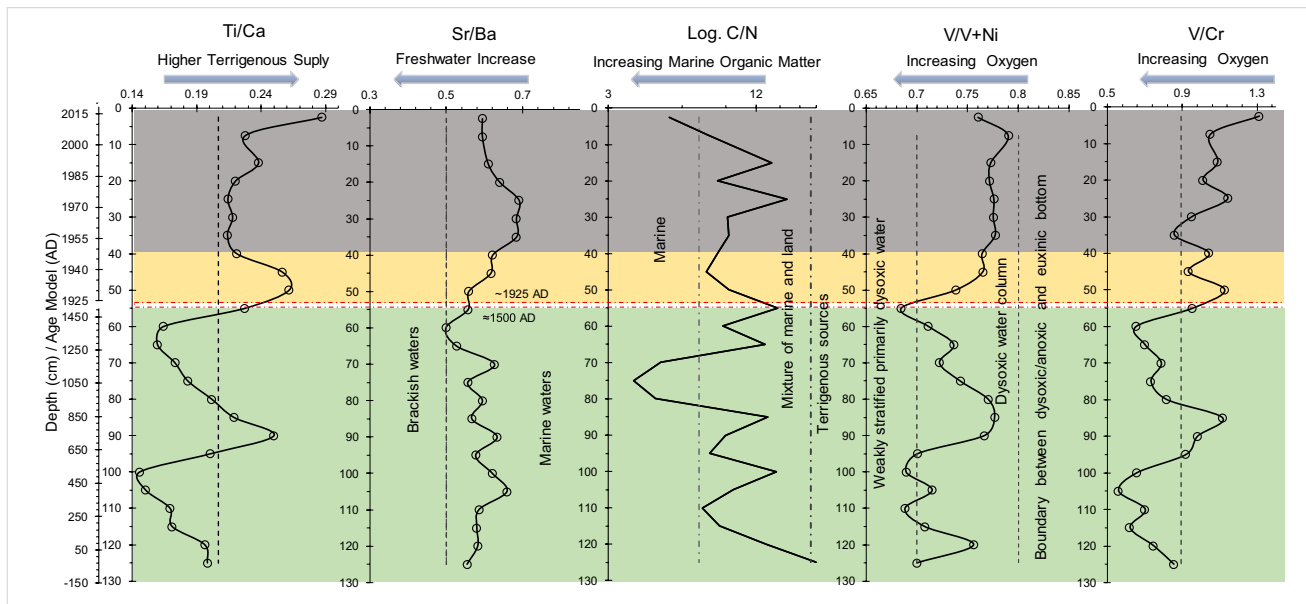


Fig. 9 Geochemical ratios used to identify sedimentological or sedimentary environmental changes. The dashed vertical line represents the average value of Ti/Ca and V/Cr, or indicative values used to interpret the results of the other variables. An age scale is represented. The yellow band marks the interval with very low foraminife-

ral density after a sedimentary discontinuity (marked with red dashes) between ~1500–1925 AD. The colored horizontal bars indicate significant temporal changes in the characteristics of the sedimentary environment

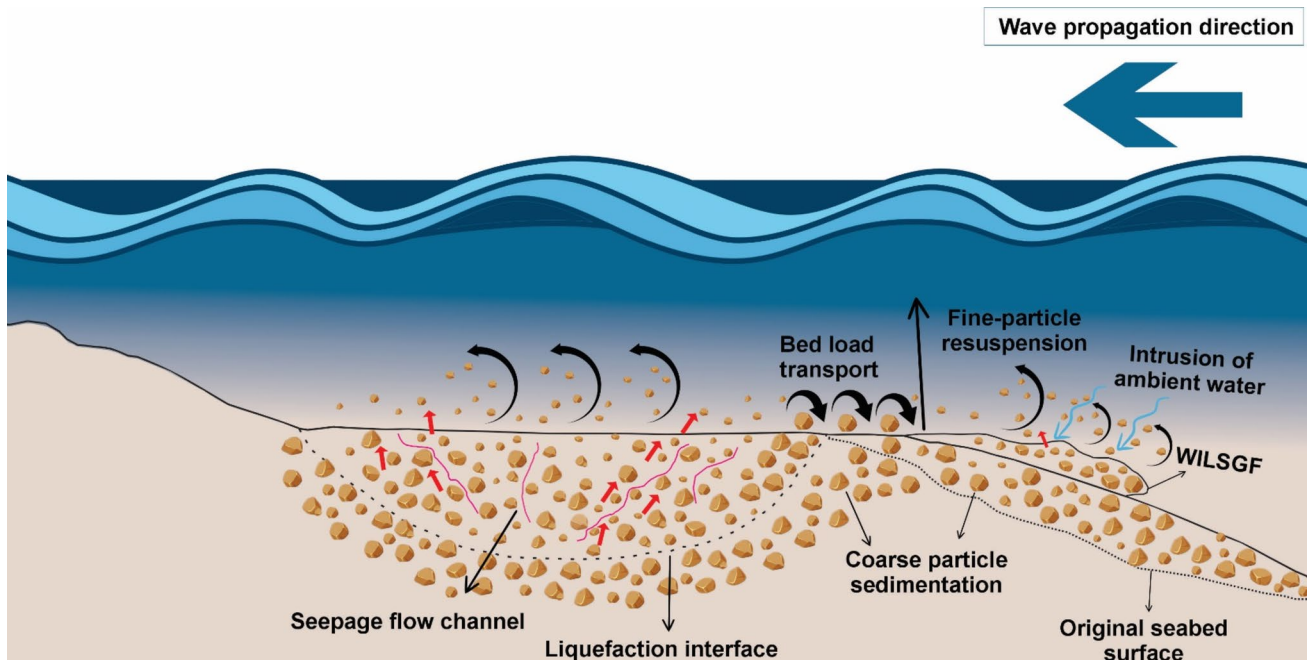


Fig. 10 Schematic representation of wave-induced liquefied sediment gravity flow according to Yu et al. (2022)

values (0.29–0.96%; $\bar{x} = 0.53 \pm 0.21\%$). TOC values increased slightly between 125–120 cm (at the base of the core), around 85 cm and in the upper part of the core (Fig. 6). The increase in TOC values in these layers

(Fig. 6) is punctuated by the rise in the V/V + Ni ratio (Fig. 9) indicating the presence of dysoxic water bottom conditions which allowed better preservation of organic matter in the sediment.

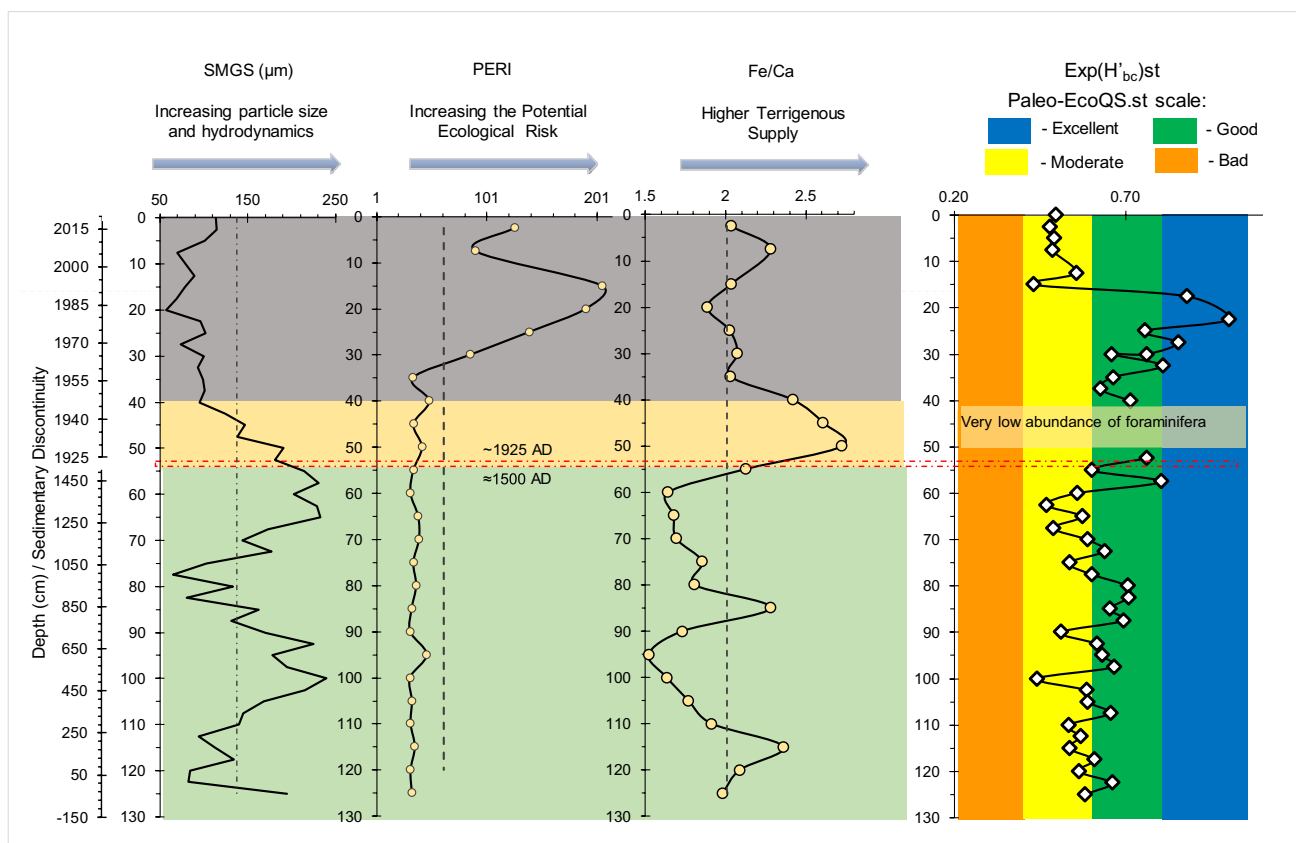


Fig. 11 Depth Plots of: SMGS (Sediment mean grain size), PERI (Potential Ecological Risk Index); Fe/Ca ratio and $\text{Exp}(H'_{bc})_{st}$ (standardized $\text{Exp}(H'_{bc})$). An age scale is represented. The dashed vertical line represents the average value of the analyzed variables. The yellow band marks the interval with very low foraminiferal density after a sedimentary discontinuity (marked with red dashes)

between ~1500–1925 AD. The colored horizontal bars indicate significant temporal changes in the characteristics of the sedimentary environment. The vertical colored bands in $\text{Exp}(H'_{bc})_{st}$ graph, represent the EcoQS scale presented in Table 1. The dotted vertical lines represent the average values of the variables for this core

Table 2 Radiocarbon Age

Core Level	SP11—92.5 cm	SP11 -122.5 cm
Beta	633,123	655,631
Material / Pretreatment	(shell): acid etch	(shell): acid etch
Conventional Age	2060 ± 30 BP	1840 ± 30 BP
Calendar Calibration Probability	95.40%	95.40%
Calendar Calibration BC/AD	409—700 cal AD	131 cal BC—215 cal AD
Calendar Calibration BP	1541—1250 cal BP	2080—1735 cal BP
IRMS $\delta^{13}\text{C}$	+1.8 ‰	+0.4 ‰
IRMS $\delta^{18}\text{O}$	-0.96 ‰	-1.5 ‰

BC, Before Christ; AD, Anno Domini; BP, Before Present

Oxygen reduction in the sediments may have been significant in some periods. The highest Mo, EF-MO, and EF-U values in the 100–65 cm interval (Fig. 7) indicate a marked oxygen reduction in the sediments (Pattan et al. 2019). On the other hand, the highest concentrations of Mn in the upper 45 cm of the core indicate the presence of oxic fronts (Martínez-Colón et al. 2017), favorable to the

chemical precipitation of this element in a general context of the prevalence of oxygen scarcity in the bottom water, as indicated by the V/V + Ni ratios (Fig. 9).

According to Emerson and Hedges (1988) and Meyers (1994), the C/N ratio indicates that values lower than seven indicate organic matter of marine origin, values > 8 and < 20 would indicate a mixture between marine and continental

organic matter, and above 20 indicate organic matter of terrigenous origin. Thus, considering the recorded C/N values in core SP11 (3.80–21.00; $\bar{x} = 9.95 \pm 4.06$) we can deduce that the organic matter deposited in the study area resulted from a mixture of continental and marine contributions. The $\delta^{15}\text{N}$ values show a range similar to that found in other Brazilian coastal systems, where there is a mixture of marine and continental materials, such as the Guanabara Bay (Senez-Mello et al. 2024), Babitonga Bay (Barros et al. 2010) and Abrolhos region (Souza et al. 2013). However, there were sharp reductions in the $\delta^{15}\text{N}$ values, for example, at 95 cm (Fig. 6), where the percentage of fine fractions was reduced (Fig. 5). The lower $\delta^{15}\text{N}$ values at the aforementioned levels may be related to the liquefaction of saturated sediment into a fluid induced by waves resulting mainly from large storms (Fig. 10; Yu et al. 2022). On the other hand, the higher $\delta^{15}\text{N}$ values may have resulted from isotopic fractionation during denitrification and the release of nitrogen gas (N_2) (Heaton 1986).

The 125–120 cm interval is marked by a decrease in foraminiferal density (Fig. 3), an increase in TOC and C/N values, and a rise in fine fractions percentage (Figs. 5, 6). These TOC and C/N increases are linked with higher values of Ti/Ca and Fe/Ca (Figs. 9, 11), indicating a more significant contribution of continental organic matter probably linked to landslides (as observed by Picullo et al. 2018) or the entry into the bay of a greater quantity of sedimentary particles of continental origin during rainy periods. These events hurt benthic foraminifera (perceived by the reduction in density and diversity). Based on these inferences, it is possible to observe records of cyclical inputs from continental sediment sources with more or less marked impacts on benthic foraminifera along the core SP11.

$\text{OM}\delta^{13}\text{C}$ values were generally low in the core's lower Section (120–55 cm; Fig. 6), indicating that organic matter from continental sources was mainly preserved in the sediments. However, the foraminifera assemblages in this Section (125–55 cm) are essentially composed of epifaunal organisms and species common in open marine settings, such as *R. williamsoni*, *Cassidulina/Globocassidulina* (*G. crassa*, *G. subglobosa*, *C. braziliensis*), *A. differens*, *S. pulchella* and *B. aculeata* (Figs. 3 and 4), indicating a broader intercommunication with the open ocean. As these organisms prefer to consume organic matter resulting from oceanic productivity with higher food quality than recalcitrant and degraded materials (with low nutritional quality) from terrestrial sources, one would expect the preserved organic matter to have resulted essentially from marine productivity. However, the greater exposure of the study area to oceanic processes did not generally favor a large accumulation of organic matter in the sediment. On the other hand, the organic matter resulting from marine productivity was probably quickly consumed by the benthic fauna, oxidized,

and has not been preserved in the sediment. In addition, the significant relative abundance of bolivinids and buliminids and *Cassidulina/Globocassidulina* throughout the core (except in section 50–40 cm; Fig. 3) might suggest that the flux of organic matter from marine sources to the bottom was significant.

The V/V + Ni ratio indicates that the bottom water was generally dysoxic between 95–65 cm and 45–0 cm intervals (Fig. 9). It can, therefore, be concluded that the TOC contents preserved in the sediment do not reflect all the carbon flux that reached the bottom; instead, the TOC was probably high but was also rapidly consumed and oxidized, leading to its low preservation in the sedimentary record; so just recalcitrant organic materials from the mainland have been preserved in the sediments as indicated by the $\text{OM}\delta^{13}\text{C}$ values (Fig. 6).

However, from 50 cm towards the core top, the progressively rising of $\text{OM}\delta^{13}\text{C}$ values suggest an increase in marine contributions associated with the deposition of fine sediments and a rise in the density and diversity of foraminifera (Figs. 3, 5, 6, 11). These data indicate that sedimentary stability (more favorable hydrodynamic conditions) and an adequate supply of high-quality organic matter, at least in the section between 40–17.5 cm, favored the development of foraminifera communities.

Indeed, the progressively rising of $\text{OM}\delta^{13}\text{C}$ values in the upper 50 cm is associated with an increase in TOC, P, N, and S (Fig. 6). The relationship between $\text{OM}\delta^{13}\text{C}$ and TOC, P, and N in this section suggests an increase in productivity in the region following the introduction of nutrients (Fig. 6). This nutrient increase may be a consequence of anthropogenic activities in the region. The association of TOC with S and the persistently high values of the V/V + Ni ratio (Figs. 6 and 9) indicate a marked decrease in oxygen levels and the production of sulfides through the degradation of organic matter in anoxic environments or microenvironments. Thus, the top of the core SP11 registers a progressive eutrophication process.

5.2 Before the industrialization

The interval between 125 and 40 cm would correspond to a record before the 1950s that marks the onset of significant expansion of urbanization in the region surrounding Sepetiba Bay. This interval was intersected with the discontinuity at ~ 50 cm. The 125–40 cm interval does not show any significant enrichment of PTEs.

The main species of benthic foraminifera between 125–40 cm (excluding the 55–40 cm sedimentary layer) were *R. williamsoni*, *E. oceanense*, *B. peruviana*, and *G. crassa*, among others. This foraminiferal assemblage composition indicates that the environmental conditions were similar to those prevailing in the inner continental shelf

(Reiss and Hottinger 1984). Thus, as mentioned, this interval registers a greater connection with oceanic processes. A similar observation was done in core SP8 (Castelo et al. 2021b), collected in the Marambaia Cove, near the study area (Fig. 1). This can be ascribed to two main reasons: according to Reis et al. (2020) and Dadalto et al. (2022), at 2000 years ago, sea level was still above the current level and Marambaia Barrier Island was not fully formed, conditions that favored a greater oceanic influence in the outer sector of Sepetiba Bay. During this interval (~125–55 cm), in which the sediments exhibited relatively low concentrations of PTEs, such as Cd and Zn, the study area was exposed to the ocean processes.

5.3 Anthropized environment

From ~40/35 cm up to 5 cm from the top, there is an increase in: fine fractions of the sediment (fine fraction, very fine and fine sand fractions; Fig. 5); concentrations of metals (i.e., Zn, Cd, Pb, and Ag); values of TOC, N, S, $\delta^{13}\text{C}_{\text{OM}}$, PLI, PERI, EF-Cd and EF-Zn (Figs. 6, 7, 11). These results are confirmed by the CoIA, where samples from this interval were related to pollution (PLI, PERI, TOC and EF-Zn).

Araújo et al. (2017b) and Silva et al. (2022a) also observed a notable increase in Zn, Cd, and Pb during this period, associated with the rapid acceleration of urbanization in the region from the mid-twentieth century onwards. The rising concentrations of PTEs are also associated with decreasing sediment mean grain size (due to the increment of coarse silt and fine and very fine sand fractions) and TOC, S, N, P, and $\delta^{13}\text{C}_{\text{OM}}$ contents. These results suggest that the increase in contamination in the study area is associated with increased eutrophication and greater oxygen scarcity due to a higher supply of organic matter (a similar remark was made by Shawar et al. (2018).

The recent evolution of Sepetiba Bay has been reasonably well studied, with several publications providing evidence of an overall increase in eutrophication and pollution in the region since the 1950s (Barcellos et al. 1997; Marques et al. 2006; Gomes et al. 2009; Castelo et al. 2021a; Silva et al. 2022a). Since then, the higher levels of environmental stress have been further increased due to engineering works in the surrounding region, such as the construction of ports (Terminal Ilha da Guaíba – 1973; Porto de Itaguaí – 1982), steelworks (Cia Siderurgica do Atlântico – 2010) and metallurgy (Cia Ingá Mercantil—1962 to 1998), as well as the development of urban, industrial and rural landscapes.

The EF values show that sediments have been significantly enriched in Cd and Zn from the 1980s onwards (Fig. 7). According to the Sutherland (2000) classification, both elements reached significant enrichment. The EF values obtained for these chemical elements increased in the upper 30 cm of the core given the accident of the Companhia Ingá

Mercantil, located on Madeira Island, which dumped about 20×10^6 tons of zinc smelting ore tailings in Sepetiba Bay (Barcellos et al. 1991).

The PERI and PLI indices exponentially grew since ~1970 (Figs. 7, 11). The PERI values in this period indicate moderate ecological risk. According to Tomlinson et al. (1980), PLI values > 1 indicate a process of environmental degradation. Higher PERI and PLI indices and more pronounced environmental degradation processes have been recorded in other areas of Sepetiba Bay (e.g., Araújo et al. 2017a, b; Castelo et al. 2021a; Silva et al. 2022a, b; Damasceno et al. 2024a, b). No contamination could be expected in the study area, given the distance of core SP11 from the primary sources of contamination, i.e., Madeira Island and the Guandú River mouth (Souza et al. 2021).

The CoIA results show, for instance, that there is a clear separation on samples from 7.5 to 40 cm (Fig. 8A) due to pollution as we can see from environmental canonical weight in Fig. 8C. At the time, some species are abundant in those samples because more related to pollution (such as *A. tepida*, *B. striatula* and *B. elegantissima*) as we can observe from faunal canonical weight in Fig. 8B. Remarkable changes in the upper core interval are also observed in the composition of the foraminiferal assemblages, such as reducing marine species (common in the nearby continental shelf). In this interval, there is a high abundance and dominance of opportunistic taxa, often related to polluted conditions, as shown by the CoIA (Fig. 8B). *Ammonia* becomes the dominant genus in the assemblages, mainly represented by *A. tepida*, *A. parkinsoniana*, and *A. buzasi* (Fig. 4). *Ammonia tepida*, which accounts for more than 40% of the assemblage in this sedimentary record, is a shallow-water infaunal species (Coccioni 2000) that proliferates mainly in coastal environments enriched with organic matter due to its high tolerance to oxygen depletion (Boltovskoy 1965; Castelo et al. 2021b).

The high relative abundance of the *Ammonia* genus, namely of *A. tepida*, indicates a change towards a more confined condition (González-Regalado et al. 2019). This inference is corroborated by other proxies, such as the exponential increase in the *Ammonia/Elphidium* ratio (Fig. 4) and the general reduction of foraminiferal density and diversity, mainly in the upper 20 cm (Fig. 3).

Ammonia buzasi an allochthonous species, was recorded in core SP11. This species, from the Caribbean Sea (Hayward et al. 2021), was found in the first half of the twentieth century in core SP11, but mainly after 1970, when it reached a relative abundance higher than 3%. The introduction of this invasive species in Sepetiba Bay can probably be ascribed to the discharge of ballast water from ships entering the region for trading (a type of activity that took place a long time ago). This is the most common way

to introduce alien foraminifera species in marine settings (Pawlowski and Holzmann 2008; Langer et al. 2012; Katsanevakis et al. 2013; Caruso and Cosentino 2014; Pavard et al. 2023).

The upper 40 cm of core SP11 (Fig. 11) should be the most distinctive period, given its relatively high concentration of PTEs, organic matter, and a unique foraminiferal assemblage. All these changes suggest a progressive alteration in the sedimentary environment, interpreted as enhanced environmental stress induced by increased confinement and pollution in the study area. On the other hand, the CoIA results also show that the healthiest, least eutrophic settings and polluted environments are punctuated by the abundance of species such as *E. excavatum*, *R. williamsoni*, *E. oceanensis*, *B. peruviana*, *S. pulchella*, *A. differens*, *B. aculeata* and *R. auberii* (Fig. 8B-C).

There is generally a significant distance between the beginning of the arrow, the position of the core layer described by the environmental data set, and the end of the arrow, the position of the same core layer related to the relative abundance of foraminifera species (Fig. 8A). This effect results from the instability of the environment caused for example by the introduction of continental detrital materials (represented for example by the increase in Ti/Ca values; Fig. 9), by post-depositional processes induced for example by wave-induced liquefied sediment gravity flow, by the deposition of foraminiferal tests from other areas of the ocean, diagenetic and taphonomic processes capable of degrading the foraminiferal tests present in the sediments, the differential destruction of foraminiferal tests. Phenomena of this kind can induce differences in the composition of the sub-recent faunas and reduce the agreement between the foraminifera assemblages present in the sediment and the characteristics of the environmental data set. However, despite these natural divergences, the results of the CoIA diagram in Fig. 8A clearly characterize the major environmental and faunal changes recorded in the core SP11.

The results presented in Fig. 11 summarize some of the leading environmental changes experienced in Sepetiba Bay. The upper 40 cm (~ 1950 to the present) records a significant increase in pollution levels caused by human activities during the last decades.

5.4 Factors driving the Paleo-EcoQS.st in the last 2000 years in the outer region of the Sepetiba Bay

Based on the $\text{Exp}(H'_{bc})$ values from core SP11 and applying the categorization of Bouchet et al. (2018), the Paleo-EcoQS exhibited good to high Paleo-EcoQS in the last ~ 2000 years (Fig. 12). This core has much better Paleo-EcoQS than core SP8, which shows a Paleo-EcoQS varying from bad to good. The worse conditions recorded in core SP8 can be ascribed

to its position inside Marambaia Cove, a more confined region (Figs. 1, 12).

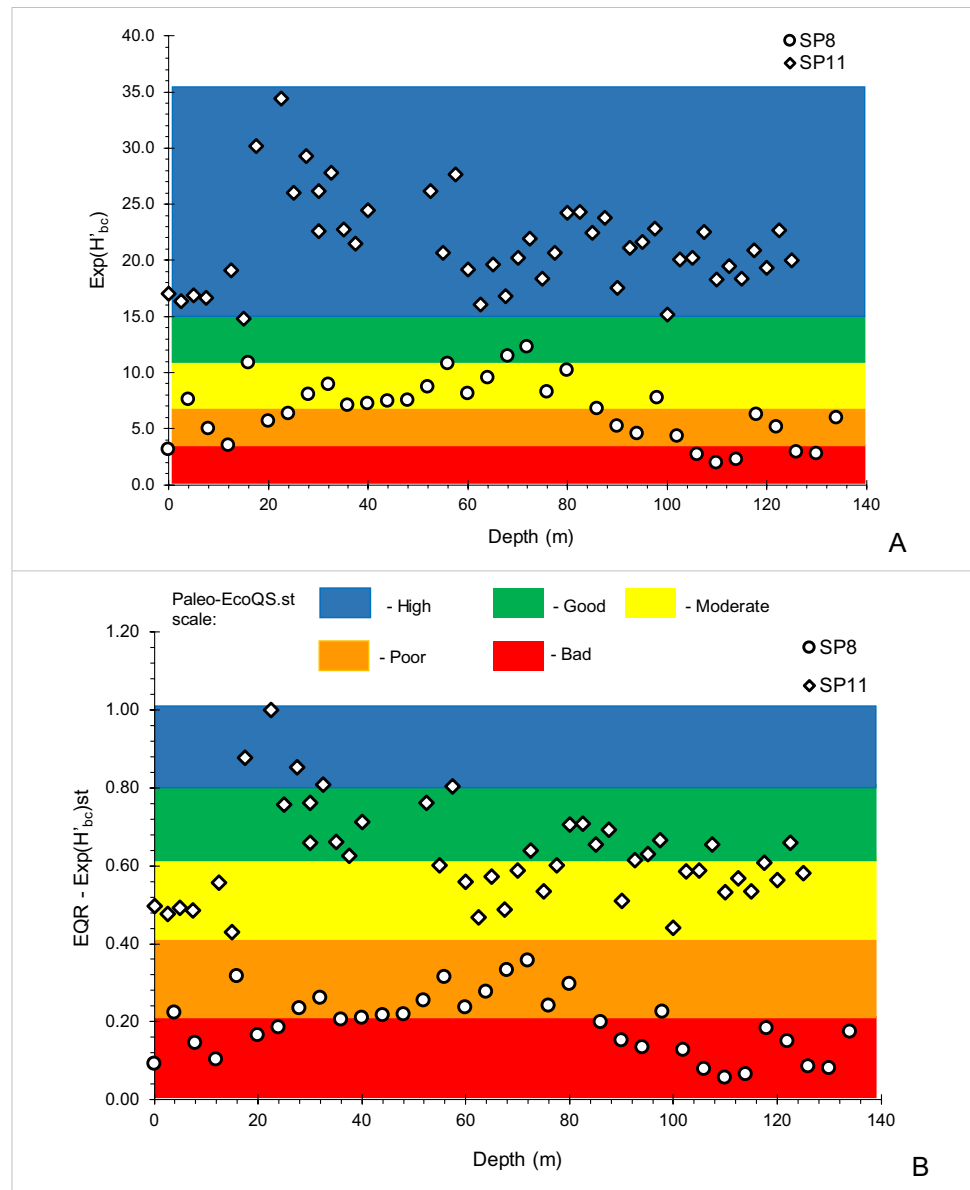
Environmental change can modify species dynamics and interactions, causing rapid changes in biodiversity at various spatial scales (Blowes et al. 2019; IPBES 2019). It is usually considered that the highest diversity of a biological community corresponds, in general, to lower environmental stress or better environmental conditions (Cleland 2011; Hong et al. 2022).

It can be expected that a coastal area impacted by anthropogenic activities had better environmental conditions in the past (Castelo et al. 2021b). So, it is predictable that the conditions of maximum environmental quality of that ecosystem have been reached before industrialization or the greatest human impact on the region. However, foraminifera are affected by factors other than pollution and eutrophication processes, such as variations in salinity, substrate stability, and hydrodynamics. So, highly dynamic and complex coastal systems may have had unfavorable conditions caused by climatic and sea level variations and the formation, consolidation or break-up of barrier islands, as noted, for example, in core SP8 (Castelo et al. 2021b).

For this reason, in core SP11, instead of taking as a reference the diversity (represented by $\text{Exp}(H'_{bc})$) from a pre-industrializing period, such as from ~ 215 AD (122.5 cm) and 1500 AD (~ 55 cm), the highest value of $\text{Exp}(H'_{bc})$ (i.e., 34.4), found at 22.5 cm deep (~ 1986 AD) was considered as the period with the best environmental conditions. Therefore, when standardizing (st) the $\text{Exp}(H'_{bc})$ values in both cores with the maximum value of this index in core SP11 (i.e., 34.4 through the EQR), it can be observed that the Paleo-EcoQS.st along the core SP11 was generally higher than those found along the core SP8 (i.e., Marambaia Cove). The environmental conditions in the core SP8 ranged from bad to poor during the Holocene, i.e., they were much worse than those estimated by Castelo et al. (2021b).

The reconstruction of the Paleo-EcoQS.st in core SP11 suggests moderate to good values before ~ 1500 AD and good to high between 1996 and 2003, and moderate tending towards bad since 2003. The decrease in Paleo-EcoQS.st from good to moderate was cyclical before ~ 1500 AD; the episodic reduction in environmental quality during this period (~ 215 AD to ~ 1500 AD) was unrelated to environmental contamination or high anthropogenic impact. In fact, textural, geochemical and foraminiferal data points to an unstable sedimentary environment that was affected by climate change (more or less rainfall, heavy storms), erosive events or introduction of terrigenous sediment during the rainiest periods, disturbances caused by the megaripple migration and wave-induced gravitational mass flows. In this context, the sedimentological instability can be seen as the leading cause of the reduction in foraminiferal diversity during this period.

Fig. 12 Comparison of $\text{Exp}(H'_{bc})$ and EQR or $\text{Exp}(H'_{bc})_{st}$ (standardized $\text{Exp}(H'_{bc})$) in cores SP8 and SP11 (Fig. 1) and the inferred Paleo-EcoQS and Paleo-Eco-QS_{st}. The $\text{Exp}(H'_{bc})$ values for core SP8 are from Castelo et al. 2021b; Fig. 1) and for the core SP11 (data from this work)



In addition, changes in the geomorphology of Marambaia Barrier Island may have also contributed to a reduction in the influence of marine processes in the region from ~1925 AD onwards. This confinement progressively favored the deposition of finer sediments. It increased the stability of the sedimentary environment, possibly favoring the development of foraminiferal populations and their biodiversity (Castelo et al. 2021b).

The decrease of the Paleo-EcoQS_{st} after 1985 (upper core layers, 15–0 cm) followed the sharp increase in the PERI (i.e., 20–15 cm), probably related to the spillage of pollutants and their release into Sepetiba Bay following the working process of Companhia Mercantil e Industrial Ingá (CIA Ingá) set in the Madeira Island, in 1962. This company processed calamine ore to produce zinc with high

purity (Magalhães et al. 2001). The company's tailings accumulated in piles on Madeira Island, rich in elements such as cadmium, zinc, mercury and lead, began to pollute the soil and water, threatening the biota and health of the region's inhabitants and degrading the natural ecosystem of the Sepetiba Bay and surrounding mangroves (Lacerda and Molisani 2006). The increase in EF-Zn and EF-Cd values from ~1965 onwards is evident in this region (Fig. 7). The CIA Ingá was Brazil's largest toxic waste contamination area (Gonçalves et al. 2020). With the company's bankruptcy in 1998, the facilities were abandoned, and the control systems were neglected, leading to the continuous contamination and risk of environmental accidents (Molisani et al. 2004; Lacerda and Molisani 2006). There have been several episodes of contamination in Sepetiba

Bay as a result of leaking dykes containing metal-contaminated tailings (Gonçalves et al. 2020). In February 1996, due to heavy rains, the company's containment dyke broke, polluting the bay with heavy metals and causing one of the largest environmental disasters in Rio de Janeiro (Lacerda and Molisani 2006). In 2002, heavy rains caused chemical waste to overflow from the company's dyke into Sepetiba Bay; in 2003, the dyke broke again, and the toxic water and mud flowed into the bay's mangroves, repeating the ecological disaster of 1996 (Lacerda and Molisani 2006).

However, the contamination in the area by metals, such as Cd, Zn and Pb, is much lower than that experienced close to the source, in the inner zone of Sepetiba Bay, near Madeira Island (Araújo et al. 2017a, b; Silva et al. 2022a). The remaining question is how the metals were transported to the region where core SP11 was retrieved.

Access to the ports is dredged in Sepetiba Bay, and several areas have been used to dispose of dredged materials (according to Rodrigues et al. 2020). Some of these areas are close to the study area (sites 1, 2 signed in Fig. 1) and in the Atlantic Ocean, located about 6.1 nautical miles from the coast (site 3; Fig. 1): Datum WGS-84 (nautical chart n° 1607), Latitude 23° 11'00" S and Longitude 43° 54' 30" W (Companhia Docas do Rio de Janeiro, 2007). Site 1 seems to have been one of the most used. Probably the disposal of contaminated dredged sediments closer to the study area after the chemical waste from the company's dyke overflowed into Sepetiba Bay in 2003 should have been the main cause of the reduction of the Paleo-EcoQS.st (by contamination by metals and silting) in the upper part of the core SP11, as was also observed in the core SP9 (Saibro et al. 2023). Dredged spoil disposal activities may have contributed to the greater enrichment of nutrients and increased coastal productivity in the outer region of the SB.

6 Conclusion

Core SP11 provided relevant information for understanding the evolution of the paleoenvironmental conditions in the outer area of Sepetiba Bay over ~2,000 years. The geomorphological configuration of Marambaia Barrier Island enabled greater exposure to oceanic processes between ~50 AD and 1500 AD (127.5–50 cm). During this period, Paleo-EcoQS.st varied from moderate to good. Between ~50 AD and 1500 AD (~127.5–50 cm), the decreasing environmental quality may have been caused by sedimentary instability, caused by the introduction of terrigenous sediment during the rainiest periods and disturbances caused by the megaregular migration and wave-induced gravitational mass flows and foraminiferal decline. This flow of sediments caused a significant reduction in foraminifera density and diversity.

The Paleo-EcoQS.st tended to improve in the study area from the 1950s to the 1990s. Greater stability at the study site, the good connection with the ocean and the distance from sources of pollution may have contributed to these good conditions; however, this more favorable period was brief, as it occurred when PTE levels were already increasing in the study area. The uppermost interval from the 1950s AD records an exponential growth in PTEs concentrations, mainly Cd and Zn. This PTE enrichment is probably related to the disposal of dredged material from the polluted areas of SB into the disposal sites near the study area.

Thus, from the ~1990s, the Paleo-EcoQS.st decreased from high to moderate in this outer area of the SB, not only due to natural factors but probably also due to the disposal of contaminated dredged material. Core SP11 also records the occurrence of an alien species, *Ammonia buzasi*, typical of the Caribbean region, must have been introduced by ballast water from ships docked in Sepetiba Bay.

Supplementary Information The online version contains supplementary material available at <https://doi.org/10.1007/s11368-024-03925-4>.

Acknowledgements The authors would like to thank the Editor and the Reviewers for their collaboration in improving the work. This paper is a contribution of the project “Anthropized Coastal Systems: Innovative Proxies for Application to Environmental Biomonitoring and Reconstitution of Quaternary Paleoenvironments” financed by the Fundação de Amparo à Pesquisa do Estado do Rio de Janeiro—FAPERJ (Edital Projetos Temáticos no Estado do Rio de Janeiro—2021, process # E-26/211.278/2021). Virginia Martins would like to thank the Conselho Nacional de Desenvolvimento Científico e Tecnológico of Brazil, CnPQ (processes # 302676/2019-8; # 305719/2023-8) for the research grants and to FAPERJ and for the research grants (processes # E-26/202.927/2019; # E-26/200.333/2023). Murilo Saibro would like to thank the CNPq (process # 141863/2023-4) for his PhD fellowship. Fabricio Leandro Damasceno would like to thank the FAPERJ for the fellowship and for ensuring the progress of this research (Process # E-26/204.093/2022). Wellen Castelo would like to thank the FAPERJ for the postdoctoral fellowship (process # E-26/205.702/2022). The authors also would like to thank the Laboratory of Micropaleontology – LabMicro/UERJ for their support in carrying out this research, the Geological Oceanography Laboratory – LabOGEO/UERJ, LGQM/UERJ, and the Sample Processing Geological Laboratory – LGPA/UERJ for their cooperation in sample processing.

Funding Open access funding provided by FCTIFCCN (b-on). Conselho Nacional de Desenvolvimento Científico e Tecnológico of Brazil, CnPQ – processes # 443662/2018–5, # 302676/2019–8, # 141863/2023–4 and #309779/2021–9. - Fundação de Amparo à Pesquisa do Estado do Rio de Janeiro—FAPERJ (Edital “PENSA RIO”, process # E-26/010.003024/2014; Edital Projetos Temáticos no Estado do Rio de Janeiro—2021, process # E-26/211.278/2021 and research grants: processes #E-26/204.093/2022, # E-26/202.927/2019, # E-26/200.333/2023, # E-26/200.427/2023.

Data availability The data supporting this work are available in tables and as supplementary materials.

Declarations

Ethical approval The authors followed the ethical standards.

Conflicts of interest The authors declare that there are no conflicts of interest.

Consent to participate Authors have consent to participate.

Consent to publish Authors have consent to publish.

Open Access This article is licensed under a Creative Commons Attribution 4.0 International License, which permits use, sharing, adaptation, distribution and reproduction in any medium or format, as long as you give appropriate credit to the original author(s) and the source, provide a link to the Creative Commons licence, and indicate if changes were made. The images or other third party material in this article are included in the article's Creative Commons licence, unless indicated otherwise in a credit line to the material. If material is not included in the article's Creative Commons licence and your intended use is not permitted by statutory regulation or exceeds the permitted use, you will need to obtain permission directly from the copyright holder. To view a copy of this licence, visit <http://creativecommons.org/licenses/by/4.0/>.

References

- Alvares CA, Stape JL, Sentelhas C, de Moraes Gonçalves JL, Sparovek G (2013) Köppen's climate classification map for Brazil. *Meteorol Z* 22(6):711–728. <https://doi.org/10.1127/0941-2948/2013/0507>
- Appleby PG, Oldfield F (1983) The assessment of ^{210}Pb data from sites with varying sediment accumulation rates. *Hydrobiologia* 103:29–35. <https://link.springer.com/content/pdf/10.1007/BF00028424.pdf>. Accessed on June 15, 2024
- Appleby PG, Oldfield F (1978) The calculation of lead-210 dates assuming a constant rate of supply of unsupported ^{210}Pb to the sediment. *CATENA* 5(1):1–8. [https://doi.org/10.1016/S0341-8162\(78\)80002-2](https://doi.org/10.1016/S0341-8162(78)80002-2)
- Araújo DF, Boaventura GR, Machado W, Viers J, Weiss D, Patchineelam SR, Ruiz I, Rodrigues APC, Babinski M, Dantas E (2017a) Tracing of anthropogenic zinc sources in coastal environments using stable isotope composition. *Chem Geol* 449:226–235. <https://doi.org/10.1016/j.chemgeo.2016.12.004>
- Araújo DF, Peres LGM, Yopez S, Mulholland DS, Machado W, Tonhá M, Garnier J (2017b) Assessing man-induced environmental changes in the Sepetiba Bay (Southeastern Brazil) with geochemical and satellite data. *C R Geosci* 349:290–298. <https://doi.org/10.1016/j.crte.2017.09.007>
- Baptista Neto JA, Gaylarde CC, Carvalho DG, Lourenço FP, Fonseca EM (2023) Occurrence of microplastics derived from tyres in bottom sediments of Guanabara Bay, Brazil: a form of pollution that is neglected or difficult to detect. *Water Emerging Contam Nanopl* 2:10. <https://doi.org/10.20517/wecn.2023.20>
- Barcellos C, Lacerda LD (1994) Cadmium and Zinc source assessment in the Sepetiba Bay and basin region. *Environ Monit Assess* 29:183–199. <https://doi.org/10.1007/BF00546874>
- Barcellos C, Rezende CE, Pfeiffer WC (1991) Zn and Cd production and pollution in a Brazilian coastal region. *Mar Pollut Bull* 22:558–561. [https://doi.org/10.1016/0025-326X\(91\)90896-Z](https://doi.org/10.1016/0025-326X(91)90896-Z)
- Barcellos C, Lacerda LD, Ceradini S (1997) Sediment origin and budget in Sepetiba Bay (Brazil) – an approach based on multielemental analysis. *Environ Geol* 32:203–209. <https://doi.org/10.1007/s002540050208>
- Barik SS, Singh RK, Hussai SM, Tripathy S, Zariqian CAA (2022) Spatial and seasonal distribution of Ostracoda in a lagoonal environment along the northeastern coast of India: Implications to assess coastal ecology and paleoenvironment. *Mar Micropaleontol* 174:102082. <https://doi.org/10.1016/j.marmicro.2021.102082>
- Barros GV, Martinelli LA, Oliveira Novais M, Ometto JP, Zuppi GM (2010) Stable isotopes of bulk organic matter to trace carbon and nitrogen dynamics in an estuarine ecosystem in Babitonga Bay (Santa Catarina, Brazil). *Sci Total Environ* 408:2226–2232. <https://doi.org/10.1016/j.scitotenv.2010.01.060>
- Birch GF (2020) An assessment of aluminum and iron in normalisation and enrichment procedures for environmental assessment of marine sediment. *Sci Total Environ* 727:138123. <https://doi.org/10.1016/j.scitotenv.2020.138123>
- Blowes SA, Supp S, Antão LH, Bates A, Bruelheide H, Chase JM et al (2019) The geography of biodiversity change in marine and terrestrial assemblages. *Science* 366:339–345. <https://doi.org/10.1126/science.aaw1620>
- Boltovskoy E, Giussani G, Watanabe S, Wright R (1980) Atlas of benthic shelf foraminifera of the Southwest Atlantic. Dr. W. Junk b.v., Publishers, The Hague, pp 147. E-book. [https://doi.org/10.1016/S0025-3227\(03\)00044-6](https://doi.org/10.1016/S0025-3227(03)00044-6)
- Boltovskoy E (1965) Los foraminíferos recientes. *Biología, métodos de estudio, aplicación oceanográfica*. Eudeba, Editorial Universitaria de Buenos Aires, pp 510
- Borges HV, Nittrouer CA (2016) Sediment accumulation in Sepetiba Bay (Brazil) during the Holocene: A reflex of the human influence. *J Sediment Environ* 1(1):90–106. <https://doi.org/10.12957/jse.2016.21868>
- Bouchet M, Alve E, Rygg B, Telford RJ (2012) Benthic foraminifera provide a promising tool for ecological quality assessment of marine waters. *Ecol Indic* 23:66–75. <https://doi.org/10.1016/j.ecolind.2012.03.011>
- Bouchet M, Goberville E, Frontalini F (2018) Benthic foraminifera to assess Ecological Quality Statuses in Italian transitional waters. *Ecol Indic* 84:130–139. <https://doi.org/10.1016/j.ecolind.2017.07.055>
- Bouchet VPM, Pavard J-C, Holzmann M, McGann M, Armynot du Châtelet E, Courleux A, Pezy J-F, Dauvin J-C, Laurent Seuront L (2023) The invasive Asian benthic foraminifera *Trochammina hadai* Uchio, 1962: identification of a new local in Normandy (France) and a discussion on its putative introduction pathways. *Aquat Invasions* 18(1):23–38. <https://doi.org/10.3391/ai.2023.18.1.103512>
- Bronk Ramsey C (2009) Bayesian analysis of radiocarbon dates. *Radiocarbon* 51(1):337–360
- Buat-Menard P, Chesselet R (1979) Variable influence of the atmospheric flux on the trace metal chemistry of oceanic suspended matter. *Earth Planet Sci Lett* 42:398–411. [https://doi.org/10.1016/0012-821X\(79\)90049-9](https://doi.org/10.1016/0012-821X(79)90049-9)
- Caruso A, Cosentino C (2014) The first colonization of the Genus *Amphistegina* and other exotic benthic foraminifera of the Pelagian Islands and south-eastern Sicily (Central Mediterranean Sea). *Mar Micropaleontol* 111:38–52. <https://doi.org/10.1016/j.marmicro.2014.05.002>
- Carvalho C, Oshiro LMY, Keuneck KA (2021) Growth and mortality analyses of the White shrimp *Penaeus schmitti* (Decapoda: Penaeidae) in Sepetiba Bay, Brazil: An exploited data-deficient species. *Reg Stud Mar Sci* 42:101641. <https://doi.org/10.1016/j.rsma.2021.101641>
- Carvalho BC, Guerra J (2020) Aplicação de modelo de tendência direcional de transporte ao Longo de uma Ilha-Barreira: Restinga da Marambaia- (RJ, SE Brasil). *Anu Inst Geocienc – UFRJ* 43(2). https://doi.org/10.11137/2020_2_101_118
- Castelo WFL, Martin MVA, Ferreira PAL, Figueira R, Cost CF, Fonseca LB, Bergamashi S, Pereira E, Terroso D, Pinto AFS, Simon MB, Socorro OAA, Frontalini F, Silva LC, Rocha F, Geraldes M, Guerra J (2021a) Long-term eutrophication and contamination of the central area of Sepetiba Bay (SW Brazil). *Environ Monit Assess* 193:100. <https://doi.org/10.1007/s10661-021-08861-1>

- Castelo WFL, Martins MVA, Martínez-Colón M, Guerra JV, Dadalto TP, Terroso D, Soares MF, Frontalini F, Duleba W, Socorro OAA, Geraldés MC, Rocha F, Bergamaschi S (2021b) Disentangling natural vs. Anthropogenic induced environmental variability during the Holocene: Marambaia Cove, SW sector of the Sepetiba Bay (SE Brazil). *Environ Sci Pollut Res* 28:22612–22640. <https://doi.org/10.1007/s11356-020-12179-9>
- Clarke A, Juggins S, Conley D (2003) A 150-year reconstruction of the history of coastal eutrophication in Roskilde Fjord, Denmark. *Mar Pollut Bull* 46(12):1615–1618. [https://doi.org/10.1016/S0025-326X\(03\)00375-8](https://doi.org/10.1016/S0025-326X(03)00375-8)
- Cleland EE (2011) Biodiversity and ecosystem stability. *Nat Educ Knowledge* 3(10):14
- Coccioni R (2000) Benthic foraminifera as Bioindicators of Heavy Metal Pollution – A case of study from the Goro Lagoon (Italy). In: Martin RE (ed) *Environmental Micropaleontology: the application of microfossils to environmental geology*. Kluwer Academic/Plenum Publishers, New York, pp 71–103
- Companhia Docas do Rio de Janeiro (2007) Dragagem dos acessos aquaviários ao Porto de Itaguaí, composto de: serviços de dragagem no Canal de Acesso Principal, Bacia de Evolução do Terminal de Minério e Rota Preferencial (denominado atualmente como canal derivativo). https://www.portosrio.gov.br/sites/default/files/inline-files/Relatorio_Dragagem_Itaguaí_2007.pdf
- Dadalto TP, Carvalho BC, Guerra JV, Rei AT, Silva CG (2022) Holocene morpho-sedimentary evolution of Marambaia Barrier Island (SE Brazil). *Quat Res* 105:182–200. <https://doi.org/10.1017/qua.2021.43>
- Damasceno FL, Alves Martins MV, Frontalini F, Pawlowski J, Cermakova K, Angeles IB, Santos LGC, Mendonça Filho JG, Francescangeli F, Senéz-Mello TM, Castelo WF, Rebouças RC, Duleba W, Mello e Sousa SH, Laut L, Antonioli L (2024) Assessment of the ecological quality status of the Sepetiba Bay (SE Brazil): When metabarcoding meets morphology on foraminifera. *Mar Environ Res* 195:106340. <https://doi.org/10.1016/j.marenvres.2024.106340>
- Damasceno FL, Alves Martins MV, Senéz-Mello TM, Mendonça Filho JG, Pereira E, Figueira R, Nascimento CA, Arruda S, Castelo WFLC, Silva LC, AIC S, Rebouças RC, Chaves H, Mahiques MM, Geraldés MC, Damasceno R, Rocha F (2024b) b) Potential ecological risk by metals in Sepetiba Bay (SE Brazil): exporting metals to the oceanic region. *J South Am Earth Sci* 141:104934. <https://doi.org/10.1016/j.jsames.2024.104934>
- Damasceno FL, Alves Martins MV, Guerra J et al (2024c) Influence of early/mid-Holocene climate change and sea level rise on a coast with barrier islands, Rio de Janeiro State, SE Brazil. *J Sediment Environ* 9:337–360. <https://doi.org/10.1007/s43217-024-00170-0>
- Dantas M (2000) Geomorfologia do Estado do Rio de Janeiro. Ministério de Minas e Energia, Secretaria de Minas e Metalurgia, CPRM – Serviço Geológico do Brasil, Brasília. <https://doi.org/10.13140/RG.2.2.32582.57923>
- Dewenter J, Yong J, Schup PJ, Löhmus K, Kröncke I, Moorathi S, Pieck D, Kuczynski L, Rohde S (2023) Abundance, biomass and species richness of macrozoobenthos along an intertidal elevation gradient. *Ecol Evol* 13:e10815. <https://doi.org/10.1002/ece3.10815>
- Diaz RJ, Rosenberg R (2008) Spreading dead zones and consequences for marine ecosystems. *Science* 321(5891):926–929. <https://doi.org/10.1126/science.1156401>
- Disaró ST, Tota VI, Watanabe S, Ribas ER, Pupo D (2022) Biodiversidade Marinha da Bacia de Potiguar: Foraminifera. Museu Nacional/UFRJ, Rio de Janeiro, p 264
- Dolédéc S, Chessel D (1994) Co-inertia analysis: an alternative method for studying species environment relationships. *Freshw Biol* 31(3):277–294
- Dray S et al (2007) The ade4 package-II: Two-table and K-table methods. *R News* 7(2):47–52
- Dreujou E, Desroy N, Carrière J, Tréau de Coeli L, McKindsey CW, Archambault P (2021) Determining the ecological status of benthic coastal communities: a case in an anthropized sub-arctic area. *Front Mar Sci* 8:637546. <https://doi.org/10.3389/fmars.2021.637546>
- Emerson S, Hedges JI (1988) Processes controlling the organic carbon content of open ocean sediments. *Paleoceanogr Paleoclimatology* 3(5):621–634. <https://doi.org/10.1029/PA003i005p00621>
- Filippos LS, Duleba W, Hohenegger J, Pregolato LA, Bouchet VMP, Alves Martins MV (2023) Domestic sewage outfall severely altered environmental conditions, foraminiferal communities and ecological quality statuses in front of the nearshore Beach of Cigarras (SE Brazil). *Water* 15(3):405. <https://doi.org/10.3390/w15030405>
- Folk RL, Ward WC (1957) Brazos River bar: a study in the significance of grain size parameters. *J Sediment Res* 27(1):3. <https://doi.org/10.1306/74D70646-2B21-11D7-8648000102C1865D>
- Ford AK, Jouffray J-B, Norström AV, Moore BR, Nuges MM, Williams GJ, Bejarano S, Magron F, Wild C, Ferse SCA (2020) Local human impacts disrupt relationships between benthic reef assemblages and environmental predictors. *Front Mar Sci* 7:571115. <https://doi.org/10.3389/fmars.2020.571115>
- Francescangeli F, Armynot du Chatelet E, Billon G, Trentesaux A, Bouchet VMP (2016) Paleo-ecological quality status based on foraminifera of Boulogne-sur-Mer harbour (Pas-de-Calais, Northeastern France) over the last 200 years. *Mar Environ Res* 117:32–43. <https://doi.org/10.1016/j.marenvres.2016.04.002>
- Gomes FC, Godoy JM, Godoy M, Carvalho ZL, Lopes RT, Sanchez-Cabez JA, Lacerda LD, Wasserman JC (2009) Metal concentrations, fluxes, inventories and chronologies in sediments from Sepetiba and Ribeira Bays: A comparative study. *Mar Pollut Bull* 59:123–133. <https://doi.org/10.1016/j.marpolbul.2009.03.015>
- Gonçalves RA, Douglas F, Rezende C, Almeida P, Lacerda L, Gamae B, Godoy J (2020) Spatial and temporal effects of decommissioning a zinc smelter on the sediment quality of an estuary system: Sepetiba Bay, Rio de Janeiro, Brazil. *J Braz Chem Soc* 31(4):683–693. <https://doi.org/10.21577/0103-5053.20190232>
- González-Regalado ML, Carro B, Arroyo M, Ruiz F, Borrego J, Abad M, Izquierdo T, Tosquella J, Prudencio MI, Dias MI, Marques R, Romero V, Vidal JR, Cáceres LM, Gómez P, Toscano A, Monge G, Carretero MI, Campos JM, Bermejo J, García EXM (2019) Distribution of benthic foraminifera in the marine estuary of the Guadalquivir River (SW Spain): a preliminary report. *Fish Oceanogr* 9(1):2. <https://doi.org/10.19080/OFOAJ.2019.09.555759>
- Govin A, Holzwarth U, Heslop D, Keelin LF, Zabel M, Mulitza S, Colling JA, Chiessi CM (2012) Distribution of major elements in Atlantic surface sediments (36°N–49°S): Imprint of terrigenous input and continental weathering. *Geochem Geophys Geosyst* 13(1). <https://doi.org/10.1029/2011GC003785>
- Håkanson L (1980) Ecological risk index for aquatic pollution control. A Sedimentological Approach. *Water Res* 14:975–1001. [https://doi.org/10.1016/0043-1354\(80\)90143-8](https://doi.org/10.1016/0043-1354(80)90143-8)
- Hayward BW, Holzmann M, Pawlowski J, Parke JH, Kaushik T, Toyofuk MS, Tsuchiya M (2021) Molecular and morphological taxonomy of living *Ammonia* and related taxa (Foraminifera) and their biogeography. *Micropaleontol* 67(2–3):109. <https://doi.org/10.47894/mpal.67.2-3.01>
- Hayward BW, Le Coze F, Vachard D, Gross O (2024) World Foraminifera Database. Accessed through: <https://www.marinespecies.org/foraminifera/>. Accessed on 11 June 2024

- Heaton THE (1986) Isotopic studies of nitrogen pollution in the hydrosphere and atmosphere: a review. *Chem Geol* 59:87–102. [https://doi.org/10.1016/0168-9622\(86\)90059-X](https://doi.org/10.1016/0168-9622(86)90059-X)
- Heaton T, Köhler P, Butzin M, Bard E, Reime R, Austin W, Skinner L (2020) Marine 20 - The Marine Radiocarbon Age Calibration Curve 0–55,000 cal BP. *Radiocarbon* 62:4:779–820. <https://doi.org/10.1017/RDC.2020.68>
- Hong P, Schmid B, De Laender F, Eisenhauer N, Zhang X, Chen H, Craven D, De Boeck HJ, Hautier Y, Petchey OL, Reich PB, Steudel B, Striebel M, Thakur MP, Wang S (2022) Biodiversity promotes ecosystem functioning despite environmental change. *Ecol Lett* 25(2):555–569. <https://doi.org/10.1111/ele.13936>
- IPBES (2019) Summary for policymakers of the global assessment report on biodiversity and ecosystem services. Intergovernmental Science- Policy Platform on Biodiversity and Ecosystem Services, Zenodo
- Irizuki T, Ito H, Sako M, Yoshioka K, Kawano S, Nomura R, Tanaka Y (2015) Anthropogenic impacts on meiobenthic Ostracoda (Crustacea) in the moderately polluted Kasado Bay, Seto Inland Sea, Japan, over the past 70 years. *Mar Pollut Bull* 91:149–159. <https://doi.org/10.1016/j.marpolbul.2014.12.013>
- Jesus MSS, Frontalini F, Bouchet VMP, Yamashita C, Sartoretto JR, Figueira RCL, Sousa SHM (2020) Reconstruction of the Paleoeological quality status in an impacted estuary using benthic foraminifera: The Santos Estuary (São Paulo state, SE Brazil). *Mar Environ Res* 162:105121. <https://doi.org/10.1016/j.marenvres.2020.105121>
- Jones B, Manning DAC (1994) Comparison of geochemical indices used for the interpretation of palaeoredox conditions in ancient mudstones. *Chem Geol* 111(1–4):111–129. [https://doi.org/10.1016/0009-2541\(94\)90085-X](https://doi.org/10.1016/0009-2541(94)90085-X)
- Katsanevakis S, Zenetos A, Belchior C, Cardoso AC (2013) Invading European Seas: Assessing pathways of introduction of marine aliens. *Ocean Coast Manag* 76:64–74. <https://doi.org/10.1016/j.ocecoaman.2013.02.024>
- Koop L, Amiri-Simkooei A, Reijnders K, O'Flynn S, Snellen M, Simons D (2019) Seafloor classification in a sand wave environment on the Dutch continental shelf using multibeam echosounder backscatter data. *Geosciences* 9(3):142. <https://doi.org/10.3390/geosciences9030142>
- Lacerda LD, Marins V., Barcellos C, Molisan MM (2004) Sepetiba Bay: a case study of the environmental geochemistry of heavy metals in subtropical Coastal Lagoon. *Environ Geochem Trop Subtrop Environ*, pp 293–318. https://link.springer.com/chapter/10.1007/978-3-662-07060-4_21
- Lacerda LD, Molisani MM (2006) Three decades of Cd and Zn contamination in Sepetiba Bay, SE Brazil: Evidence from the mangrove oyster *Crassostrea rhizophorae*. *Mar Pollut Bull* 52(8):974–977. <https://doi.org/10.1016/j.marpolbul.2006.04.007>
- Langer MR, Weinmann AE, Lötters S, Rödder D (2012) “Strangers” in Paradise: Modeling the biogeographic range expansion of the foraminifera *Amphistegina* in the Mediterranean Sea. *J Foraminifer Res* 42(3):234–244. <https://doi.org/10.2113/gsjfr.42.3.234>
- Laut L, Vilar A, Belart P, Clemente I, Fontana L, Pereira E, Ballalai J (2020) Organic matter compounds as a tool for trophic state characterization in a hypersaline environment: Araruama Lagoon. *Brazil J South Am Earth Sci* 97:102403. <https://doi.org/10.1016/j.jsames.2019.102403>
- Laut L, Vilar A, Carelli T, Sambugaro J, Martins MA, Fontana PB, Laut L (2024) Living benthic foraminifera and organic matter compounds as proxies to characterize the trophic state in an impacted hypersaline environment: Araruama Lagoon – Brazil. *J South Am Earth Sci* 137:104842. <https://doi.org/10.1016/j.jsames.2024.104842>
- Li Q, Pei L, Huang Z, Shu W, Li Q, Song Y, Zha H, Schäfer M, Nordhaus I (2023) Ecological risk assessment of heavy metals in the sediments and their impacts on bacterial community structure: A case of study of Bamen Bay in China. *Mar Pollut Bull* 186:114482. <https://doi.org/10.1016/j.marpolbul.2022.114482>
- Liu B, Mastalerz M, Schieber J, Teng J (2020) Association of uranium with macerals in Marine Black Shales: Insights from the upper Devonian New Albany Shale. *Illinois Basin Int J Coal Geol* 217:103351. <https://doi.org/10.1016/j.coal.2019.103351>
- Loeblich AR, Tappan H (1987) Foraminiferal genera and their classification. Van Nostrand Reinhold, New York, p 970
- Loring DH (1991) Normalization of heavy-metal data from estuarine and coastal sediments. *ICES J Mar Sci* 48:01–115
- Magalhães VF, Carvalho CEV, Pfeiffer WC (2001) Arsenic contamination and dispersion in the Engenho Inlet, Sepetiba Bay, SE, Brazil. *Water Air Soil Poll* 129:83–90
- Magurran AE (1988) *Ecological Diversity and Its Measurement*. University Press, Princeton, NJ
- Marques AN, Monna F, Silva Filho EV, Fernex FE, Simões Filho FFL (2006) Apparent discrepancy in the contamination history of a sub-tropical estuary evaluated through ²¹⁰Pb profile and chronostratigraphical markers. *Mar Pollut Bull* 52:532–539. <https://doi.org/10.1016/j.marpolbul.2005.09.048>
- Martínez-Colón M, Hallock P, Green-Ruiz C, Smoak J (2017) Temporal variability in potentially toxic elements (PTE's) and Benthic foraminifera in estuarine environment in Puerto Rico. *Micro-paleontol* 63(6):357–382. <https://doi.org/10.47894/mpal.63.6.01>
- Martins K, Brito E, Freitas JCO, Quirino MR, Oliveira JBL, Silva EBS (2019) Assessment of the anthropogenic influence on contamination level present in Vitória's Bay – Espírito Santo Brazil. *City Environ Interact* 4:100030. <https://doi.org/10.1016/j.cacint.2020.100030>
- Martins MVA, Hohenegger J, Martínez-Cólon M, Frontalini F, Bergamashi S, Laut L, Belart P, Mahiques M, Pereira E, Rodrigues R, Terroso D, Miranda P, Geraldies MC, Villena HH, Reis T, Socorro OAA, Mello e Sousa SH, Yamashita C, Rocha F (2020) Ecological quality status of the NE sector of the Guanabara Bay (Brazil): A case of living benthic foraminiferal resilience. *Mar Pollut Bull* 158:111449. <https://doi.org/10.1016/j.marpolbul.2020.111449>
- Meyers PA (1994) Preservation of elemental and isotopic source identification of sedimentary organic matter. *Chem Geol* 114:289–302. [https://doi.org/10.1016/0009-2541\(94\)90059-0](https://doi.org/10.1016/0009-2541(94)90059-0)
- Milnes AR, Fitzpatrick RW (1989) Titanium and zirconium minerals. In: Dixon JB, Weed SB (eds) *Minerals in Soil Environment*, 2nd edn. Soil Sci Soc Am, Madison, WI, pp 1131–1205
- Molisani MM, Marins RV, Machado W, Paraquetti H, Bidone ED, Lacerda LD (2004) Environmental changes in Sepetiba Bay, SE Brazil. *Reg Environ Change* 4:17–27. <https://doi.org/10.1007/s10113-003-0060-9>
- Niencheski LF, Windom HL, Smith R (1994) Distribution of particulate trace metal in Patos Lagoon estuary (Brazil). *Mar Pollut Bull* 28:96–102. [https://doi.org/10.1016/0025-326X\(94\)90545-2](https://doi.org/10.1016/0025-326X(94)90545-2)
- Nunes M, Alves Martins MV, Frontalini F, Bouchet VMP, Francescangeli F, Hohenegger J, Figueira R, Senez-Mello TM, Castelo WFL, Damasceno FL, Laut L, Duleba W, Mello e Sousa SH, Antonioli L, Geraldies MC (2023) Inferring the ecological quality status based on living benthic foraminiferal indices in transitional areas of the Guanabara Bay (SE Brazil). *Environ Pollut* 320:121003. <https://doi.org/10.1016/j.envpol.2023.121003>
- Pattan JN, Parthiban G, Amonkar A (2019) Productivity controls on the redox variation in the southeastern Arabian Sea sediments during the past 18 kyr. *Quat Int* 523:1–9. <https://doi.org/10.47894/mpal.63.6.01>

- Pavard JC, Richirt J, Seuront L, Blanchet H, Foue MPA, Humber S, Gouillieux B, Duong G, Bouchet VMP (2023) The great shift: The non-indigenous species *Ammonia confertitesta* (Foraminifera Rhizaria) outcompetes indigenous *Ammonia* species in the Gironde estuary (France). *Estuar Coast Shelf Sci* 289:108378. <https://doi.org/10.1016/j.ecss.2023.108378>
- Pawlowski J, Holzmann M (2008) Diversity and geographic distribution of benthic foraminifera: a molecular perspective. *Int J Biodivers Conserv* 17:317–328. <https://doi.org/10.1007/s10531-007-9253-8>
- Piciullo L, Calvello M, Cepeda JM (2018) Territorial early warning systems for rainfall-induced landslides. *Earth Sci Res* 179:228–247. <https://doi.org/10.1016/j.earsirev.2018.02.013>
- Pinto AFS, Ramalho JCM, Borghi L, Carelli TG, Plantz JB, Pereira E, Terroso D, Santos WH, Geraldles MC, Rocha F, Rodrigues MAC, Laut L, Martins MA (2019) Background concentrations of chemical elements in Sepetiba Bay SE Brazil. *J Sediment Environ* 4:108–123. <https://doi.org/10.12957/jse.2019.40992>
- Powell WG, Johnston PA, Collom CJ (2003) Geochemical evidence for oxygenated bottom waters during deposition of fossiliferous strata of the Burgess Shale Formation. *Palaeogeogr Palaeoclimatol Palaeoecol* 201(3–4):249–268. <https://doi.org/10.1016/S0031-01820300612-6>
- Raposo D, Frontalini F, Clemente I et al (2022) Benthic foraminiferal response to trace elements in a tropical mesotidal Brazilian estuary. *Estuaries Coasts* 45:2610–2631. <https://doi.org/10.1007/s12237-022-01095-5>
- REFCOND (2003) Reference Conditions for Inland Surface Waters (REFCOND) and Typology and Classification Systems of Transitional and Coastal Waters (COAST) (refer to WFD CIS Guidance Document N°s 10 and 5, respectively). https://environment.ec.europa.eu/topics/water/water-framework-directive_en Accessed on June 15, 2024
- Reis AT, Amendola G, Dadalt TP, Silv CG, Poço RT, Guerra JV, Martins V, Cardia RR, Gorini C, Rabineau M (2020) Arquitetura e evolução deposicional da sucessão sedimentar Pleistoceno Tardio-Holoceno (últimos ~20 Ka) da Baía de Sepetiba (RJ). *Rev Geoci Unesp* 39(3):695–708. <https://doi.org/10.5016/geociencias.v39i03.14366>
- Reiss Z, Hottinger L (1984) The Gulf of Aqaba – Ecological micropaleontology studies. Springer-Verlag, Berlin, Heidelberg
- Rodrigues SK, Machado W, Guerra JV, Geraldles M, Morale S, Vinzón SB (2020) Changes in Cd and Zn distribution in sediments after closure of an electroplating industry, Sepetiba Bay. *Brazil Mar Pollut Bull* 161:111758. <https://doi.org/10.1016/j.marpolbul.2020.111758>
- Rudorff NM, Bonetti CHC, Bonetti Filho J (2012) Suspended shellfish culture impacts on the benthic layer: A case study in Brazilian subtropical waters. *Braz J Oceanogr* 60(2):219–232. <https://doi.org/10.1590/S1679-87592012000200012>
- Saibro MB, Martin MVA, Guerra J et al (2023) Transfer of industrial contaminants from the inner to the outer region of Sepetiba Bay (SE Brazil) by dredge spoil dumping activities: a temporal record. *Environ Earth Sci* 82:560. <https://doi.org/10.1007/s12665-023-11259-6>
- Sandra F, Carcedo MC (2013) Benthic Community and Climate Change. In Arias AH Menéndez MC (eds.) *Marine Ecology in a Changing World*, 1st edn, Science Publishers/CRC Press/Taylor Francis, p 270. <https://doi.org/10.1201/b16334>
- Santos ALF, Ponte L, Peixoto RS, Rosman PA, Rosman CC (2018) Projeto Baías do Brasil Baías da Ilha Grande e Sepetiba – RJ. SisBaHia, Sistema Base de Hidrodinâmica Ambiental, COPPE – Engenharia Costeira e Oceanográfica, UFRJ. https://www.baiaodobrasil.coppe.ufrj.br/assets/relatorios/rel_ilhagrande_sepetiba.html, Accessed October 2024
- Senez-Mello TM, Alves Martins MV, Ferreira PAL, Figueira R, Castelo WFL, Damasceno FL, Hohenegger J, Pereira E, Duleba W, Gerarde MC (2024) Assessment of anthropogenic pollution in Guanabara Bay (SE Brazil) through biogeochemical data and stable isotope mixing models. *Environ Sci Pollut Res* 31:32972–32997. <https://doi.org/10.1007/s11356-024-33144-w>
- Shannon CE (1948) A mathematical theory of communication. *Bell Syst Tech J* 27:379–423 and 623–656
- Shawar L, Halevy I, Said-Ahmad W, Feinstein S, Boyko V, Kamyshny A, Amrani A (2018) Dynamics of pyrite formation and organic matter sulfurization in organic-rich carbonate sediments. *Geochim Cosmochim Acta* 24:219–239. <https://doi.org/10.1016/j.gca.2018.08.048>
- Silva LC, Alves Martins MV, Castelo WFL, Saibro MB, Rangel D, Pereira E, Bergamaschi S, Sousa SHM, Varela J, Laut L, Frontalini F, Chaves H, Reis AT, Aguilera O, Zaaboub N, Cheriyan E, Geraldles MC (2022a) Trace metals enrichment and potential ecological risk in sediments of the Sepetiba Bay (Rio de Janeiro, SE Brazil). *Mar Pollut Bull* 177:113485. <https://doi.org/10.1016/j.marpolbul.2022.113485>
- Silva LC, Alves Martins MV, Figueira R, Frontalini F, Pereira E, Senez-Mello TM, Castelo WFL, Saibro MB, Francescangeli F, Mello e Sousa SH, Bergamaschi S, Antonioli L, Bouchet VMP, Terroso D, Rocha F (2022) Unraveling Anthropocene paleoenvironmental conditions combining sediment and foraminiferal data: proof-of-concept in the Sepetiba Bay (SE, Brazil). *Front Ecol Evol* 10:852439. <https://doi.org/10.3389/fevo.2022.852439>
- Soares MF, Alves Martins MV, Castelo WFL et al (2024) Species richness of living foraminifera in Sepetiba Bay (SE Brazil): a species checklist. *J Sediment Environ* 9:397–417. <https://doi.org/10.1007/s43217-024-00173-x>
- Song Y, Guo Y, Liu H, Zhang G, Zhang X, Thangaraj S, Sun J (2022) Water quality shifts the dominant phytoplankton group from diatoms to dinoflagellates in the coastal ecosystem of the Bohai Bay. *Mar Pollut Bull* 183:114078. <https://doi.org/10.1016/j.marpolbul.2022.114078>
- Sonkoly J, Kelemen A, Valkó O, Deák B, Kiss R, Tóth K, Miglécz T, Tóthmérész B, Török P (2019) Both mass ratio effects and community diversity drive biomass production in a grassland experiment. *Sci Rep* 9:1848. <https://doi.org/10.1038/s41598-018-37190-6>
- Souza JRB, Costa AB, Azevedo AEG, Santos THR, Spano S, Lentini CAD, Bonagama TJ, Silva RO, Novotny EH, Zucchi MDR (2013) Carbon and nitrogen stable isotope compositions of organic matter in marine sediment cores from the Abrolhos region: indicators of sources and preservation. *Geochim Brasiliensis* 27(1):13–23. <https://doi.org/10.5327/Z0102-980020130010002>
- Souza AM, Rocha DS, Guerra JV, Cunha BA, Martins MVA, Geraldles MC (2021) Metal concentrations in marine sediments of the Rio de Janeiro Coast (Brazil): A proposal to establish new acceptable levels of contamination. *Mar Pollut Bull* 165:112113. <https://doi.org/10.1016/j.marpolbul.2021.112113>
- Sutherland RA (2000) A comparison of geochemical information obtained from two fluvial bed sediment fractions. *Environ* 39:330–341. <https://doi.org/10.1007/s002540050012>
- Swarnalatha K, Letha J, Ayoob S (2013) Ecological Risk assessment of a tropical lake system. *J Urban Environ Eng* 7(2):323–329
- Tholen K, Pätz T, Yizhaq H, Katra I, Kroy K (2022) Megaripple mechanics: bimodal transport ingrained in bimodal sands. *Nat Commun* 13:162. <https://doi.org/10.1038/s41467-021-26985-3>
- Tomlinson DL, Wilson JG, Harris CR, Jeffrey DW (1980) Problems in the assessment of heavy-metal levels in estuaries and the formation of a pollution index. *Helgol Meeresunters* 33:566–575
- Tsikopoulou I, Moraitis ML, Geropoulos A, Papadopoulou KN, Papageorgiou N, Plaiti W, Smith CJ, Karakassis I, Eleftheriou

- A (2019) Long-term changes in the structure of benthic communities: Revisiting a sampling transect in Crete after 24 years. *Mar Environ Res* 144:9–19. <https://doi.org/10.1016/j.marenvres.2018.11.008>
- Tsujimoto A, Nomura R, Yasuhara M, Yamazaki H, Yoshikawa S (2006) Impact of eutrophication on shallow marine benthic foraminifers over the last 150 years in Osaka Bay, Japan. *Mar Micropaleontol* 60:258–268. <https://doi.org/10.1016/j.marmicro.2006.06.001>
- Van de Bund W, Solimini A (2007) Ecological Quality Ratios for Ecological Quality Assessment in Inland and Marine Waters. European Commission reports 23
- Vilela CG, Figueira BO, Macedo MC, Baptista Neto JA (2014) Late Holocene evolution and increasing pollution in Guanabara Bay, Rio de Janeiro, SE, Brazil. *Mar Pollut Bull* 79:175–187. <https://doi.org/10.1016/j.marpolbul.2013.12.020>
- Wang A, Wang Z, Liu J, Xu N, Li H (2021) The Sr/Ba ratio response to salinity in clastic sediments of the Yangtze River Delta. *Chem Geol* 559:119–923. <https://doi.org/10.1016/j.chemgeo.2020.119923>
- Wang Z, Saebi M, Grey EK, Corbett JJ, Chen D, Yang D, Wan Z (2022) Ballast water-mediated species spread risk dynamics and policy implications to reduce the invasion risk to Mediterranean Sea. *Mar Pollut Bull* 174:113285. <https://doi.org/10.1016/j.marpolbul.2021.113285>
- Yu H, Liu Y, Yang L, Li W, Gao H, Wu R, Li X (2022) Characteristics of the sediment gravity flow triggered by wave-induced liquefaction on a sloping silty seabed: an experimental investigation. *Front Earth Sci* 10:909605. <https://doi.org/10.3389/feart.2022.909605>
- Yuan F, Ding Y, Wang Y, Yu W, Zou X, Chen H, Fu G, Ding D, Tang J, Tang X, Zhang Z, Li S, Li D (2021) Microplastic pollution in *Larimichthys polyactis* in the coastal area of Jiangsu. *China Mar Pollut Bull* 173:113050. <https://doi.org/10.1016/j.marpolbul.2021.113050>
- Zalán PV, Oliveira JAB (2005) Origin and structural evolution of the Cenozoic Rift System of Southeastern Brazil. *Bol Tec Petrobras* 13(2):269–300

Publisher's Note Springer Nature remains neutral with regard to jurisdictional claims in published maps and institutional affiliations.

Authors and Affiliations

Murilo Barros Saibro¹  · Maria Virgínia Alves Martins^{1,2}  · Rubens Figueira³ · Egberto Pereira¹ · Heitor Evangelista⁴ · Marcus Vinícius Licínio⁵ · Josefa Varela Guerra⁶  · Felipe de Castro Figueiredo Simões^{1,6} · Vincent Marcel Pierre Bouchet⁷ · Fabio Francescangeli⁸ · Fabrizio Fontalini⁹  · Paulo Alves de Lima Ferreira³ · Ana Beatriz Ramos de Oliveira¹  · Fabricio Leandro Dasmaceno¹  · Thaise Senez-Mello¹  · Grazielle Arantes Reis¹  · Silvia Helena Mello Sousa³  · Rodolfo Dino¹ · Antonio Tadeu dos Reis⁶  · João Wagner de Alencar Castro¹⁰ · Fernando Rocha²

✉ Maria Virgínia Alves Martins
virginia.martins@ua.pt

Murilo Barros Saibro
saibrobarros@gmail.com

Rubens Figueira
rfigueira@usp.br

Egberto Pereira
egberto@uerj.br

Heitor Evangelista
evangelista.uerj@gmail.com

Marcus Vinícius Licínio
mv.ufes@gmail.com

Josefa Varela Guerra
josefa@uerj.br

Felipe de Castro Figueiredo Simões
felipe.simoese@uerj.br

Vincent Marcel Pierre Bouchet
vincent.bouchet@univ-lille.fr

Fabio Francescangeli
fabio.francescangeli85@gmail.com

Fabrizio Fontalini
fabrizio.frontalini@uniurb.it

Paulo Alves de Lima Ferreira
paulo.alves.ferreira@hotmail.com

Ana Beatriz Ramos de Oliveira
anabeatrizramosdeoliveira@gmail.com

Fabricio Leandro Dasmaceno
fabricioldamasceno16@gmail.com

Thaise Senez-Mello
thaise_senez@id.uff.br

Grazielle Arantes Reis
grazielle.arantes93@gmail.com

Silvia Helena Mello Sousa
smsousa@usp.br

Rodolfo Dino
dinouerj@gmail.com

Antonio Tadeu dos Reis
tadeu.reis@gmail.com

João Wagner de Alencar Castro
castro@mn.ufrj.br

Fernando Rocha
tavares.rocha@ua.pt

¹ Faculdade de Geologia, Universidade do Estado do Rio de Janeiro, UERJ, São Francisco Xavier, 524, Sala 4037F, Maracanã, Rio de Janeiro, RJ 20550-013, Brazil

² GeoBioTec, Departamento de Geociências, Universidade de Aveiro, Campus de Santiago, 3810-193 Aveiro, Portugal

³ Instituto Oceanográfico, Pça. do Oceanográfico, Universidade de São Paulo, USP, 191, Butantã, São Paulo 05508-120, Brazil

⁴ Laboratório de Radioecologia e Mudanças Globais, LARAMG, Universidade do Estado do Rio de Janeiro, UERJ, Instituto de Biologia Roberto Alcântara Gomes, IBRAG, Rua São Francisco Xavier, 524, Rio de Janeiro, MaracanãRJ 20550-013, Brazil

⁵ Departamento de Ciências Fisiológicas, Centro de Ciências da Saúde, Universidade Federal do Espírito Santo, UFES, CCS, Avenida Marechal Campos, Maruípe, Vitória, ES 1468, Brazil

⁶ Faculdade de Oceanografia, Universidade do Estado do Rio de Janeiro, UERJ, Rua São Francisco Xavier, 524, 4 Andar, Bloco E, Sala 4018, Rio de Janeiro, RJ 20550-013, Brazil

⁷ UMR 8187, LOG, Laboratoire d’Océanologie et de Géosciences, UniLille, CNRS, IRD, UniLittoral Côte d’Opale, Station Marine de Wimereux, 59000 Lille, France

⁸ Department of Geosciences, University of Fribourg, Chemin Du Musée 6, 1700 Fribourg/Freiburg, Switzerland

⁹ Department of Pure and Applied Sciences, Università degli Studi di Urbino “Carlo Bo”, 61029 Urbino, Italy

¹⁰ Universidade Federal do Rio de Janeiro, Museu Nacional, Quinta da Boa Vista s/n, São Cristovão, Rio de Janeiro, RJ 20940-040, Brazil